

THE EXTENDED MORPHOLOGY OF ULTRALUMINOUS RADIO CORES

BRIAN PUNSLY

4014 Emerald Street, No. 116, Torrance, California 90503

Received 1993 December 6; revised 1994 May 27

ABSTRACT

This article investigates the extended radio morphology of a large sample of extremely powerful quasar radio cores. It is found that the extended emission is on the order of weak FRII luminosity for the most part even though the sources are at high redshift, the average redshift of the sample is 1.84. Furthermore, the sources in this catalog were observed with a dynamic range between 500 and 10 000 with the VLA, yet 30% of them are naked cores. It is argued through map morphology and polarimetry data that the sources with the strongest extended emission are dominated by Doppler enhanced beamed kiloparsec scale jets. If viewed near the sky plane, even these sources, would have weak FRII luminosities, at best.

1. INTRODUCTION

This paper is an investigation of the extended emission of ultraluminous quasar radio cores. An ultraluminous core is defined to have a core power, P_c , larger than 10^{46} ergs/s in the quasar rest frame between 10 MHz and 250 GHz assuming $H_0=55$ km/s/Mpc and $q_0=0$. These sources were chosen to minimize the selection biasing due to beaming angle, since it is argued in Sec. 2 that within a large sample most of these cores are being viewed essentially end on and statistically significant statements concerning intrinsically strong cores can be made. To be considered for the survey, a source must have been observed in the VLA A array with a dynamic range larger than 500 and $P_c \geq 10^{46}$ ergs/s (of course, one also needs to know the redshift to compute P_c). 134 such sources were found and P_c is within a factor of 10 for over 90% of the sources and within a factor of 20 for over 98% of the sample. Such a tight clustering suggest that the sample is drawn from the top end of a luminosity distribution.

The extended emission surrounding compact flat spectrum radio cores has been studied for nearly 15 years. Blandford & Königl (1979) proposed these radio cores were the jets which supply energy to extended lobe emission seen end on. This suggested the "unification scheme" that FRII radio galaxies, steep spectrum quasars, and compact radio quasars are all drawn from the same parent population, but oriented at varying angles to the line of sight [see Barthel (1989) and Antonucci (1993) for more details].

With the advent of high dynamic range, high resolution multielement arrays came evidence for the unification scheme. Perley *et al.* (1980, 1982), and Browne *et al.* (1982) found some strong radio cores surrounded by extended emission.

Observations confirming this scenario continued to be published. Antonucci & Ulvestad (1985) looked at all the known blazars at that time (~ 50) with the VLA and found most to have extended structure. The sample contained many BL Lacs with low redshift or no redshift. The distribution for the power of the extended luminosity showed that the intrinsic extended powers were less than those in the 3C catalog. However, they were close enough so that one could argue that this was merely a selection effect associated with the

fact that the 3C sample was defined at 178 MHz.

Browne & Perley (1986) analyzed the visibilities of 135 flat spectrum cores originally chosen as potential VLA calibrators in Perley (1982). Two-thirds of the sources had extended structure on a scale larger than 2 arcsec. They believed that very little of the extended emission was beamed (contrary to what is found for ultraluminous cores). The authors felt that the extended luminosity distribution was consistent with the unified scheme.

A larger sample of 250 core dominated quasars was studied in Hutchings *et al.* (1988), Neff *et al.* (1989), and Neff & Hutchings (1990). The sources were selected from the Dixon catalog and have a redshift range of 0.6–3.7. The extended morphology was studied for evolutionary effects. It was shown that the core dominance increased with redshift and the linear size decreased.

Kollgaard *et al.* (1990) and Kollgaard *et al.* (1992) examined limited samples of strong radio cores and BL Lacs, respectively. They found that the quasars tended to have FRII luminosities with prominent one-sided jets. While the BL Lacs had, generally, FRI level luminosities at low redshift, and for $z \sim 1$ the extended luminosities and morphology become borderline between FRI and FRII. As was found in Antonucci & Ulvestad (1985), BL Lacs, unlike quasar cores, can exhibit core-halo morphology (the structure inferred by the unified scheme to be common).

O'Dea *et al.* (1988) used high resolution VLA imagery of 16 core dominated quasars to study the jets. They found them to be one-sided and mildly relativistic, estimating the flow speed as $\beta \geq 0.2-0.7$.

The conclusion was that the jet and hot spot velocities might be a substantial fraction of the initial jet velocity seen on very long baseline interferometer (VLBI) scales. The matching of VLBI scales to VLA scales is an important part of the unification scheme since these are two ends of the putative conduit for energy from the central engine to the radio lobes. VLBI maps for 21 of the ultraluminous cores in this catalog exist. However, some (especially in the southern hemisphere) are merely unresolved cores. The rest exhibit one-sided jets, a few are aligned with the VLA jets such as

0836+710 (consistent with the unification scheme). There are also quite a few with position angles near 90° relative to the VLA jet. The jets tend to bend a lot making it hard sometimes to connect it up to the VLA jet if there is an unmapped gap. The maps as a whole are representative of the bimodal distribution of relative position angle peaking at 0° and 90° discussed in Conway & Murphy (1993).

In Browne & Perley (1986), and in the unified scheme in general, all flat spectrum quasars are treated on the same footing. In this article an attempt is made to delineate the intrinsically strongest cores from the rest of the sample. Only about 20% of the Antonucci & Ulvestad (1985) sample qualifies for this catalog. On average, the intrinsic core powers are one to two orders of magnitude larger than in Antonucci & Ulvestad (1985) and Browne & Perley (1986). Thus, it is not surprising that some different conclusions are reached. The most basic unified scheme asserts that the extended emission on average is independent or possibly scales with core strength. Thus, it becomes relevant to look at the intrinsically strongest cores to see if the extended emission is comparable to that of steep spectrum quasars in the same redshift range.

It was found that most sources would be classified as weak FRIIs based on the strength of extended emission alone. They rank from 2 to 4 orders of magnitude weaker than the strongest steep spectrum sources in the same redshift range (Barthel *et al.* 1988). There is a distinct subsample with strong extended emission that would have moderate FRII luminosities based on extended emission. They have one to two orders of magnitude less extended emission than the strongest steep spectrum quasars in the same redshift range. Much of this article is concerned with the study of this subsample in Sec. 4. It turns out that the extended morphology of these sources is invariably a one-sided kiloparsec scale jet. It is argued based on assumed near bilateral intrinsic symmetry that these jets are most certainly enhanced by Doppler factors larger than ten. It is clear that this subsample differs in extended luminosity from the rest of the sample by this beamed jet alone. If viewed near the sky plane, about 5% of the sources would qualify for the 5C catalog. The more powerful extended emission is found associated with radio cores clustered at high redshift, $1.5 < z < 3.0$ with the average of the subsample $\bar{z} = 2.35$. In this redshift range, $z > 1.5$, a study of steep spectrum sources was published in Barthel *et al.* (1988). If viewed near the sky plane only one source would have been luminous enough for that study and it would have ranked 81st or lower out of 90 in intrinsic power. It would also be two orders of magnitude weaker than the most powerful sources in the same redshift range.

Even at dynamic ranges as large as 500 to 10 000 a major fraction ($\sim 1/3$) of the sources are naked cores. It can also be argued that there are no core-halo objects, or if loosely interpreted at most a couple. It is highly suggestive that there is a lack of strong halo or lobe emission from the objects which dissipate intensely in a very compact region, or else the luminosity distribution for extended emission is incredibly steep and 134 is not a large sample to have a good chance of finding powerful lobes.

In Sec. 2, a rigorous definition of the intrinsic beamed core power (power of the jet defined in the rest frame of the quasar), P_c , is established. It is also argued based on a simple beaming model that it is plausible that most of the cores have similar unbeamed intrinsic powers. Furthermore, most if not all of the unresolved core jets lie within a few degrees from the line of sight. Thus, the sample would appear to be mainly similar objects, intrinsically, viewed with similar Doppler enhancement, as opposed to a random mix of strong sources seen at large angles to the line of sight and much weaker sources seen end on. This is one interesting aspect of choosing ultraluminous cores as opposed to flat spectrum cores in general.

Section 3 similarly describes a consistent definition of the extended luminosity in the quasar rest frame, P_E . The strongest sources of extended emission are discussed in Sec. 4. The maps and notes for these sources appear in the Appendix if they were available. It is shown that the emission is generally dominated by a jet in these instances, argued to be greatly Doppler enhanced.

2. RADIO CORE LUMINOSITIES

The definition of the radio core is ambiguous since it depends on the resolution and the frequency of measurement. The best choice would be unresolved emission from objects observed with the VLBI at 5 GHz. However, not enough observations have been made on ultraluminous cores to compile a statistically interesting sample. A best compromise between resolution and a large database is to define a core as the radio emission which is unresolved by the VLA in the A array at 5 GHz (an angular size between $0.4''$ and $0.7''$). Even with this compromise, many objects in this catalog were not observed with enough resolution. Observations in L band typically between 1.5 to 1.6 GHz, were considered resolved enough for this study (resolutions on the order of $1.3''$). Even at $1.3''$ resolution, emission on smaller scales can be ascertained by the deviation of the core shape from that of the beam (so-called core-extended objects). It should be remembered throughout that small scale emission less than $0.6''$ in extent might be missed for those sources observed only at 1.5 GHz and this is a shortcoming for the database. This will not be considered crucial to the data analysis, since the emphasis is on the morphology of the more extended structure. The missed extended emission is generally the base of a kiloparsec scale jet or the entire length of a short jet (probably a projection effect due to being observed nearly end on). Thus, core fluxes could be slightly overestimated at 1.5 GHz. As a final note on the core definition, core-extended objects at 5 GHz are considered resolved in this study.

One of the improvements on the classification of core strength made in this study is the use of integrated cosmological rest frame radiated power, P_c , instead of rest frame spectral luminosity at a particular frequency. A study of well over 350 core dominated objects which preceded the compilation of this catalog revealed a large discrepancy, in most cases, between assuming a flat spectrum and actually computing the energy flux associated with the spectral shape. Since over 90% of the objects in the catalog have P_c 's within

a factor of 10, assuming a flat spectra would randomize P_c enough to destroy any correlation with other quasar parameters. It was noted in this regard that most “flat spectrum” sources turnover between 5 and 20 GHz.

The question arises as to which rest frame frequencies define the domain of emission of the core. To answer this question accurately, one needs extensive high frequency data above 100 GHz. This does not exist, in particular for the fainter, high z sources. In practice, data points at 31.4 GHz or higher were found for over 85% of the sources. For many lower redshift sources ($z < 2$), it was felt that extrapolating the spectra above 250 GHz in the quasar rest frame was a reach. Thus, P_c was found by integrating the spectral luminosity from 10 MHz to 250 GHz in the quasar rest frame, even though a high frequency cutoff of 350 GHz would have ensured that the spectra of all but a few sources would have turned over. Hopefully, the sample is large enough that the randomization of P_c due to the high frequency cutoff is not critical.

Another issue to be addressed is what about sources for which there is no spectral data above 10.7 GHz. After studying many spectra of core dominated objects, a “typical” default spectrum was chosen for these: flat below 10 GHz in the earth frame and a spectral index of $\alpha = 0.33$ above 10 GHz ($S_\nu = S_0 \nu^{-\alpha}$, where S_ν is the monochromatic flux). Again, this will introduce some randomization of the P_c distribution in the sample. For instance, this spectra typically yields on the order of 70% of the power of a flat spectra for objects in this sample.

A major concern is the variability of the core. Frequency points taken at different epochs will distort the spectra. In fact, it turns out that an inverted spectrum at high frequency (above 10 GHz) is invariably due to this effect. Fortunately, simultaneous high frequency data (20–111 GHz) exists for the majority of the sample (Edelson 1987; Teräsanta *et al.* 1993; Owen *et al.* 1980; Tornikoski *et al.* 1993). This is decisive because the spectral index at high frequency is the dominant parameter for determining the power in the core. When a source is known to vary in flux, the data points are averaged to obtain a mean luminosity. This approach is limited as there are not enough data points for most sources to get a true average over time. Again, this effect will randomize the distribution of P_c within the sample.

The belief is that enough information is available to make a meaningful assessment of core power through this large sample of 134 objects, plus the many objects which were rejected due to insufficient core strength. The considerations above do nothing to account for beaming. It is hoped that, by choosing ultraluminous cores, that these objects must be very close to being viewed end on.

The core power should obey a bivariate distribution depending on intrinsic power as well as the Doppler enhancement factor. It is conjectured that for an object to make this catalog it must be near the high end of luminosity distribution in both Doppler enhancement and intrinsic luminosity. This is indirectly verified by P_c being within a factor of 10 for over 90% of the sources and within a factor of 15 for over 98% of the sample. This statement can be made more rigorous if one compares the distribution of P_c in the sample

with a simple beaming model, namely the cores are a standard candle viewed from different angles. Assume the maximum observable luminosity for the distribution, L_{\max} , is 1.43×10^{47} ergs/s (i.e., a source beamed along the line of sight). This corresponds to the source 1351–018 which ranks third in the sample in terms of core power (see Table 1). The two brightest cores, 0642+449 and 0438–436 have P_c 's much larger than the rest of the catalog so they are not considered to belong to the same distribution. We consider the 130 remaining sources $\geq 10^{46}$ ergs/s. It is assumed that the radiating plasma in the standard candle has the same bulk flow velocity for all sources. Then in analogy to Lind & Blandford (1985) if the radiation is from an unresolved continuous jet with $\alpha = 0.3$, one can find the probability that a source observed at a random angle to the line of sight will have a luminosity greater than L , $P(L)$. Our analysis is different in that we are considering luminosities in the quasar rest frame (not the frame of the beam) as opposed to monochromatic fluxes measured at earth at a fixed distance.

$$P(L) = \mathcal{P}_0 \left[\left(\frac{L_{\max}}{L} \right)^{1/(3+\alpha)} - 1 \right].$$

If $\mathcal{P}_0 = 0.711$, one has a partial luminosity distribution normalized so that $P(10^{46} \text{ ergs/s}) = 1.000$. Figure 1 plots the percent of the sample of 130 larger than or equal to the luminosity given on the horizontal axis compared to the theoretical curve $P(L)$. The fit is better than expected considering the oversimplified model and is consistent with there being no obvious selection effects which dominate the sample. In many of the individual samples from which it is drawn there are, but it might be such a varied mix of effects that no single one tends to dominate. An even better fit is seen if $L_{\max} = 1.22 \times 10^{47}$ ergs/s, corresponding to the fourth strongest source, 2126–158. Finally, if one uses the average bulk flow Lorentz factor for core dominated quasars of 11 found by Padovani & Urry (1992), one finds that all sources are within 5.75° to the line of sight in this oversimplified model. More than likely, these cores are much more energetic than the sample used in Padovani & Urry (1992) and a larger Lorentz factor would imply even a smaller spread in angle to the line of sight. For instance if $\gamma = 20$ then the maximum angle to the line of sight is 3.1° . Thus, it is possible that most of these sources are very powerful intrinsically and are at very small angles to the line of sight, as conjectured.

The unknown degree of beaming (bulk flow Lorentz factors, angle to the line of sight, beam geometry, etc.) will randomize P_c from its intrinsic value by factors of 2 or more quite easily. It is likely that when all of the randomizing effects are combined, correlations with other quasar parameters will be masked. However, these efforts at defining P_c are not wasted since many unknowns will likely cancel each other out by random chance and it seems probable that the vast majority of these objects have intrinsic P_c 's within a factor of 10. The intrinsic P_c according to most beaming studies and from determinations of bulk Lorentz γ -factors for the jetted beam on VLBI scales is probably on the order of 10^{43} ergs/s for the majority of these sources (Ghisellini *et al.* 1993).

TABLE 1. The luminosity of the extended radio structure, P_E , for a sample of ultraluminous radio cores. The table is arranged by rank of the core power, P_c , uncorrected for possible Doppler beaming. The columns are described in the text.

Rank	Source	P_c (10^{46} ergs/sec)	P_E (10^{44} ergs/sec)	R	z	ν_{\max}	Ref. E	Ref. C
1	0642+449	27.7	< 2.00	>1,384	3.402	--	e	2,3,4,6
2	0438-436	23.1	27.8	83.1	2.85	31.4	c	2,3,18
3	1351-018	14.3	< 3.00	>477	3.71	31.4	e	3,9
4	2126-158	12.2	10.2	120	3.27	--	e	1,5,7
5	1442+101	12.1	< 2.00	>605	3.53	--	a	1,5,9
6	0834-201	12.0	< 1.00	>1,200	2.75	--	e	1,3,7,19,e
7	2134+004	10.9	0.574	1,900	1.936	--	a	1,4,5,6
8	0106+013	10.6	48.0	22	2.107	--	a,f,g	
9	0014+813	10.4	3.31	316	3.41	--	x	5,10
10	0212+735	10.2	< 1.00	>1,020	2.37	--	z	1,5
11	2223-052	10.0	140	7.14	1.404	--	B,j,m,n,op	1,4,7
--	(3C446)	--	--	--	--	--	--	--
12	0528+134	9.79	3.64	269	2.06	--	b	1,6
13	1116+128	9.02	30	30	2.118	--	a	1,6
14	0836+710	8.65	12.2	71	2.160	--	a,i	1,6,18
15	0458-020	8.28	31.8	26	2.29	--	e,u,C	1,5
16	2037+511	8.13	46.5	17.5	1.69	--	d,i	3,5,13,19
--	(3C418)	--	--	--	--	--	--	--
17	0229+132	8.03	22.2	36	2.065	--	a	1,6
*	1402+044	7.87	< 3.00	> 218	3.202	--	h	7,h
18	2121+053	7.85	0.378	2,070	1.88	--	a	2,3,5,6
19	2005+403	7.71	< 1.00?	> 772	1.74	--	d	3,4,6
20	2136+141	7.59	< 1.00	> 759	2.427	--	a,e	1,5
21	1502+106	6.88	1.73	398	1.833	--	a	1,5,6
22	2251+158	6.80	7.83	86	0.859	--	a	1,4,5
--	(3C454.3)	--	--	--	--	--	--	--
23	2048+312	6.65	< 2.00	> 333	3.18	5	e	3,e
24	1633+382	6.57	2.33	282	1.814	--	a	1,4,6
25	0827+423	6.56	0.602	1,090	2.046	--	c	11,12
26	1614+051	6.29	< 2.00	>3.15	3.21	5	e	3,e
27	0537-286	5.78	2.74	211	3.11	--	c	1,5
28	1148-001	5.77	5.00	115	1.982	--	b	1,6,7,14
29	0237-233	5.59	< 1.00	> 559	2.22	--	e	1,5
30	0335-122	5.20	< 2.00	> 260	3.45	5	e	3,e
31	1555+001	5.12	< 1.00	> 512	1.722	--	b	1,5
32	2351-154	5.08	14.9	34.1	2.67	31.4	e	2,3
33	0319+121	4.90	3.46	142	2.67	31.4	a	1
34	0917+449	4.87	6.87	71	2.18	--	e	2,6
35	1032-199	4.86	8.95	54	2.198	--	b	1,7,19
36	2145+067	4.78	0.242	1,980	0.99	--	a	1,4,6
37	1354-122	4.77	3.29	145	1.89	--	b	1,6,7
38	1624+416	4.70	12.7	37	2.55	31.4	i	1
39	0153+744	4.55	< 1.00	> 455	2.338	--	b	1,5,10
40	2227-088	4.48	< 1.00?	> 448	1.56	--	d	1,5,7
41	0146+056	4.10	< 1	> 410	2.345	--	a	1,5
42	0234+285	4.04	2.62	112	1.207	--	a	1,6
43	0457+024	3.99	< 1	> 399	2.384	--	a	1,5
44	0434-188	3.96	< 1	> 396	2.702	--	b	1,5,9
45	0528-250	3.91	3.51	111	2.812	--	c	1,5,7,9
46	0420-014	3.84	0.256	1,500	0.915	--	k	1,4,6,7
47	1253-055	3.81	8.63	41	0.540	--	j,q,s	1,4,6
--	(3C279)	--	--	--	--	--	--	--
48	1638+398	3.69	1.00	369	1.67	--	b	1,6
49	1127-145	3.66	2.84	128	1.187	--	b	1,7
50	0400+258	3.59	0.144	2,490	2.109	--	a	1,5,11
51	1705+018	3.56	< 1.00	> 356	2.57	8.1	e	2,17,e
52	0136+176	3.53	8.30	42.5	2.73	5	e	2,3,e
53	0537-441	3.51	0.274	1,280	0.894	--	c	1,20
54	1730-130	3.50	3.98	87	0.902	--	c,r	3,16,19
55	1616+063	3.47	9.55	36	2.09	10.7	e	2,3
56	0833+385	3.34	3.29	102	2.101	--	a	1
57	1741-038	3.33	< 1.00	> 333	1.057	--	b	1,6,7
58	2223+210	3.25	4.23	76.7	1.959	--	a	1,5
59	1124+571	3.21	< 1.00	> 321	2.89	10.7	e	2,3
60	1548+056	3.08	< 0.50	> 616	1.422	--	a	1,5
61	1333+459	2.97	< 1.00	> 297	2.45	10.7	e	2
62	2310+385	2.91	< 1.00	> 291	2.17	5	e	e
63	1641+399	2.77	4.32	64	0.594	--	a,t	1,6
--	(3C345)	--	--	--	--	--	--	--
64	1936-155	2.76	< 1.00?	> 276	1.66	--	d	1,7
65	0149+335	2.75	22.5	12.2	2.43	10.7	e	2,3
66	0202-172	2.75	< 1.00?	> 275	1.74	--	d	1,7
67	1611+343	2.71	0.745	364	1.401	--	a	1,6
68	1021-006	2.64	4.53	58.2	2.55	8.1	e	3,17
69	0048-071	2.52	7.50	33.6	1.97	5	d	3,d
70	2320-035	2.42	< 1.00	> 242	2.04	5	e	3,e
71	0119+247	2.33	7.89	30	2.03	--	e	11,e
72	0333+321	2.28	1.41	162	1.263	--	a,i	3,4,6,19
73	2230+114	2.25	4.74	48	1.037	--	a	1,4,6
74	0917+624	2.20	0.249	884	1.44	--	a	1,6
75	1656+477	2.08	< 0.50	> 416	1.622	--	a	2,3
76	0235+164	2.05	0.407	504	0.94	--	a	1,4,11
77	0149+218	2.03	0.772	263	1.32	--	a	1,6
78	0736-063	2.03	2.78	73	1.91	5	d	3,d
79	0805+046	2.02	24.4	8.4	2.877	8.1	h,w	3,17,h
80	1954+513	2.01	7.48	26.9	1.23	--	b,f	1,5,6
81	0112-017	2.00	2.61	77	1.365	--	d	1,6
82	1308+326	1.99	1.02	194	0.996	--	a,y	1,4,6
83	0923+392	1.94	4.10	47	0.698	--	a,f	1,4
84	1739+522	1.93	0.67	288	1.38	--	b	1,5
85	0237-027	1.88	0.210	893	1.38	--	c	11,12
86	1406-076	1.85	< 1.00	>1.85	1.494	--	b	1,7
87	1705+188	1.84	< 1.00	> 184	2.57	8.1	e	3,17
88	1020+191	1.80	11.5	15.6	2.14	5	e	3,e

TABLE 1. (continued)

Rank	Source	P_c (10^{46} ergs/sec)	P_E (10^{44} ergs/sec)	R	z	v_{max}	Ref. E	Ref. C
89	0414-189	1.80	< 1.00?	> 180	1.54	--	d	1,6
*	2254+024	1.74	< 2.00	> 87	2.09	8.1	h	3,17,h
90	0336-019	1.73	1.28	135	0.85	--	v	1,7
91	0938+119	1.73	17.9	9.7	3.19	5	e	3,e
92	0804+499	1.72	0.203	847	1.433	--	a	1
93	2044-168	1.72	9.7	17.8	1.937	5	d	3,19,5
94	0119-046	1.72	35.9	4.8	1.95	5	d	3,e
95	0859-140	1.69	2.1	80.2	1.327	--	b,i	1,6
*	1331+170	1.69	< 2.00	> 85	2.081	5	h	3,h
96	1150+812	1.67	0.656	255	1.25	--	a	1,5
97	0133+476	1.67	< 1.00	> 167	0.86	--	b	1,4,6,11
98	1055+018	1.64	1.82	90.1	0.89	--	a	1,4,5
99	0707+476	1.61	2.85	56.5	1.31	--	a	1
100	1328+307	1.59	0.797	199	0.846	--	z,A	1,A
--	(3C286)	--	--	--	--	--	--	--
101	1049+215	1.58	3.66	43	1.30	--	b	1,5
102	1551+130	1.58	9.01	17.5	2.21	--	e	2,3,12
103	0258+058	1.55	12.2	12.7	2.31	5	e	3,e
104	1039+811	1.55	0.648	239	1.26	--	b	1,5,10
105	2216-038	1.54	2.13	72	0.901	--	b	1,5,7
106	1008-159	1.48	< 1.00	> 148	1.18	--	b,d	1,5,7
107	2328+107	1.46	1.06	137	1.49	--	a	1,5
108	0054-006	1.46	3.99	37	2.77	5	e	3,e,w
109	0605-085	1.43	1.89	75	0.87	--	b,i	1,6,7
110	0215+015	1.42	4.70	30.2	1.72	--	k	2,3,17,21
111	0122-003	1.40	< 1.00	> 140	1.07	--	b,d	1
112	1606+106	1.39	0.681	204	1.23	--	a	1,6
113	0859+470	1.37	12.0	11.4	1.462	--	a,r,s	1,6
114	1243-072	1.37	0.266	514	1.287	--	b	1,5,7
115	1144+402	1.36	0.038	3,580	1.01	--	a	2,6
116	0448-187	1.34	3.25	41	2.05	5	e	3,e
117	2329-162	1.33	2.96	45	1.153	--	b	1,5
*	1225+317	1.33	< 2.00	> 67	2.23	5	h	3,h,w
118	0711+356	1.32	0.233	590	1.62	--	a	1,5
119	0830+115	1.30	20.7	6.3	2.97	5	e	3,e
120	0202+319	1.25	< 0.50	> 250	1.466	--	a	1,6
121	1807+279	1.23	17.6	7.0	1.76	--	d	2,3,12
122	0748-126	1.20	< 1.00	> 120	0.889	--	b	1,6
123	1504-167	1.20	< 1.00	> 120	0.876	--	b	1,6,7
124	1328+254	1.16	< 1.00	> 116	1.055	--	A	1,5,A
--	(3C287)	--	--	--	--	--	--	--
125	2253+417	1.15	< 0.50	> 230	1.476	--	a	2,3,12
126	1145-071	1.15	< 1.00	> 115	1.345	--	b	1,5,7
127	1455+348	1.10	7.21	15.2	2.73	1.5	e	e
128	1642+690	1.07	2.80	38	0.751	--	a,f	1,6
129	0945+408	1.06	2.55	42	1.252	--	a	1,4,5
130	0650+371	1.01	< 1.00?	> 101	1.982	--	d	2,3,12
131	2249+185	1.01	10.9	9.27	1.76	15	d,w	3,d,A
--	(3C454)	--	--	--	--	--	--	--
132	0812+332	1.01	12.2	8.3	2.43	5	e	3,e
133	0248+430	0.975	0.399	244	1.316	--	b	d
134	0406-127	0.954	1.07	89	1.563	5	d	3,d

References to TABLE 1

- | | |
|--|--|
| <p>Extended Emission</p> <p>a) Murphy, Browne and Perley 1933</p> <p>b) Browne and Perley 1986</p> <p>c) Browne and Murphy 1987</p> <p>d) Neff, Hutchings and Gower 1989</p> <p>e) Neff and Hutchings 1990</p> <p>f) Kollgaard <i>et al.</i> 1990</p> <p>g) Kollgaard <i>et al.</i> in preparation</p> <p>h) Feigelson <i>et al.</i> 1984</p> <p>i) O'Dea <i>et al.</i> 1988</p> <p>j) Browne <i>et al.</i> 1982</p> <p>k) Antonucci and Ulvestad 1985</p> <p>l) Antonucci <i>et al.</i> 1986</p> <p>m) Ulvestad <i>et al.</i> 1983</p> <p>n) Antonucci 1986</p> <p>o) Browne <i>et al.</i> 1981</p> <p>p) Simon <i>et al.</i> 1985</p> <p>q) De Pater and Perley 1983</p> <p>r) Perley <i>et al.</i> 1980</p> <p>s) Perley <i>et al.</i> 1980</p> <p>t) Kollgaard <i>et al.</i> 1990</p> <p>u) Briggs <i>et al.</i> 1989</p> <p>v) Hutchings <i>et al.</i> 1988</p> <p>w) Barthel <i>et al.</i> 1988</p> <p>x) Kuhr <i>et al.</i> 1986</p> <p>y) Kollgaard <i>et al.</i> 1992</p> <p>z) Pearson, Perley and Readhead 1985</p> <p>A) Van Bruegel <i>et al.</i> 1992</p> <p>B) Fejjes <i>et al.</i> 1992</p> <p>C) Briggs (unpublished)</p> | <p>Core Emission</p> <p>1) Kuhr <i>et al.</i> 1981</p> <p>2) Kuhr <i>et al.</i> 1979</p> <p>3) Véron-Cetty and Véron 1991</p> <p>4) Teräsranca, H. <i>et al.</i> 1992</p> <p>5) Steppe <i>et al.</i> 1988</p> <p>6) Edelson 1987</p> <p>7) Tornikoski <i>et al.</i> 1993</p> <p>8) Chini <i>et al.</i> 1989</p> <p>9) Geldzahler and Witzel 1981</p> <p>10) Geldzahler and Kuhr 1983</p> <p>11) Owen <i>et al.</i> 1980</p> <p>12) Owen <i>et al.</i> 1978</p> <p>13) Landaou <i>et al.</i> 1978</p> <p>14) Abraham <i>et al.</i> 1984</p> <p>15) Owen and Mufson 1977</p> <p>16) Wiren <i>et al.</i> 1982</p> <p>17) Willard <i>et al.</i> 1979</p> <p>18) Chini <i>et al.</i> 1988</p> <p>19) Perley 1982</p> <p>20) M. Tornikoski, private communication 1993</p> <p>21) R. Chini, private communication 1993</p> |
|--|--|

Since most “flat spectrum core” spectra turn over, it became ambiguous to discriminate against steep spectrum cores, SSCs. It was hard to say that an object which turns over at 4 GHz with $\alpha=0.6$ was intrinsically different from one that turns over at 8 GHz with $\alpha=.45$. In fact there seems to be a continuous distribution in turnover points and high frequency spectral indices. Those normally considered SSCs are at the “tail end” of the bivariate distribution. Very few SSCs appear in the sample because a steep spectral index at high frequencies usually equates to small intrinsic powers. There are a few SSC powerhouses at high z such as 1442+101 and 0237–233, both are naked cores.

3. EXTENDED EMISSION

The observations on extended structure come from a variety of references. However, over three-fourths of the objects come from either Murphy *et al.* (1993), Browne & Perley (1986), Neff *et al.* (1989) or Neff & Hutchings (1990). Sources were observed at different frequencies with varying degrees of sensitivities by each research team. Those observations at 1.5–1.6 GHz are superior for detecting extended emission on scales larger than 1". However, as mentioned before, they sometimes fail to resolve small scale jet structures which appear on 5 GHz maps. The nature of this problem is put in perspective by the example of 0014+810 which is unresolved at a dynamic range of 500 at 1.5 GHz by Neff & Hutchings (1990). However, by sitting on the object for 6 h at higher frequency revealed a faint small jet, 3.3 mJy at 5 GHz and nothing at other frequencies (Kuhr *et al.* 1986). This may be commonplace for many other high redshift ($z > 2$) naked cores, if one could perform such lengthy observations. Conversely, observations at 5 GHz tend to resolve out diffuse emission, especially at high redshift. In spite of these shortcomings, the data from different observers is fairly consistent. Many of the objects have been studied by more than one group. In all but a few instances the measured extended emission agree within a factor of two.

In order for the reader to judge the conclusions drawn from the data, it is necessary to compare and contrast the main references used to determine the extended powers, P_E . Murphy *et al.* (1993) used the A, B, and C arrays for a total of 30–45 min at 1.6 GHz to form hybrid maps with dynamic ranges from 5000 to 10 000. This is the best large sample on extended emission larger than 1". However, small jet structure less than 1" can be missed as evidenced by 1624+416 (O’Dea *et al.* 1988). Browne & Perley (1986) and Browne & Murphy (1987) used early snap shot data at 1.5 GHz in the A-array on which Perley (1982) was based. However, the data were carefully reanalyzed to achieve a dynamic range of 1000 by studying visibility plots. Again, the resolution is only 1.3" meaning that small jets might be missed. These results agree with Murphy *et al.* (1993) and Neff *et al.* (1989) to within a factor of 2 in almost all cases.

Neff *et al.* (1989) is a study of sources with $1 < z < 2$ using the A-array at 5 GHz. Excellent data on jets is obtained with a resolution on the order of 0.5". A dynamic range of 600 was obtained. Very diffuse extended structure is sometimes resolved out as in the case of 0215+015 (Antonucci &

Ulvestad 1985). Neff & Hutchings (1990) is a similar survey for $z > 2$. The lower z sources in the survey were observed at both 5 and 1.5 GHz in the A-array. The high z sources were observed at only 1.5 GHz. A dynamic range on the order of 500 was achieved.

Kollgaard *et al.* (1990) and O’Dea *et al.* (1988) provide high dynamic range, high resolution maps of limited samples at 5 GHz in the A-array. The other references contribute only one or two sources to the survey. The best situation is when both L band and C band A-array data are available so that one can see small scale jets as well as large scale diffuse emission. However, this usually is not the case. It is believed that the 134 sources in this catalog have been observed appropriately for this study. It is acknowledged that occasionally a small scale jet or very diffuse emission is missed. But the large sample size should overwhelm these shortcomings in statistical analyses.

The computation of intrinsic extended luminosity, P_E , is complicated by the lack of spectral information—there is usually only one frequency of observation or two measurements with different sensitivities to diffuse emission often yielding very steep spectral indices [the second situation was prevalent in the early days of the VLA, see Perley *et al.* (1980) and Perley *et al.* (1982)]. Since a significant fraction of the emission is in jets and hot spots with spectral indices typically from 0.5 to 0.8 (Bridle & Perley 1984) and diffuse lobe emission has spectral indices typically from 0.7 to 1.1 (Kellerman *et al.* 1969), a compromise spectral index of 0.7 was chosen for all sources. Clearly, this can yield an estimate of total extended power only reliable to within a factor of 2 or 3. Since steep spectrum objects can have spectra which turnover at low frequencies [usually at less than 200 MHz, Kellerman *et al.* (1969) and Kuhr *et al.* (1981)] a low frequency cutoff of 10 MHz in the quasar rest frame is chosen for the extended emission. To be consistent with the calculation of P_c , a high frequency cutoff of 250 GHz is implemented so one can compute the parameter $R \equiv P_c/P_E$. It is noted that the spectra of lobe emission often steepens at high frequency (Kellerman *et al.* 1969 and Kuhr *et al.* 1981). Without access to spectral information on the extended emission, this cannot be pursued here. The basic hope is that the large data base will statistically average out the expediences taken in calculating P_E .

A major point previously not considered significant in earlier studies of extended emission of core dominated objects is how much of the extended structure is Doppler enhanced by beaming? (Browne & Perley 1986 and Antonucci & Ulvestad 1985.) In the majority of this sample, the extended structure has a significant contribution from a one-sided jet-like region. This is in contrast to a study of lobe dominated 3C objects selected on the basis of steep spectrum emission in which jet luminosities are usually very small compared to lobe emission (Bridle 1993). At higher redshifts than the 3C sample, the importance of jets in steep spectrum quasars was observed in Barthel *et al.* (1988). However, consistent with the unified model of radio sources, one finds higher jet prominence in this core dominated sample than in the Barthel *et al.* (1988) sample, on the average.

However, inconsistent with the beaming hypothesis is the

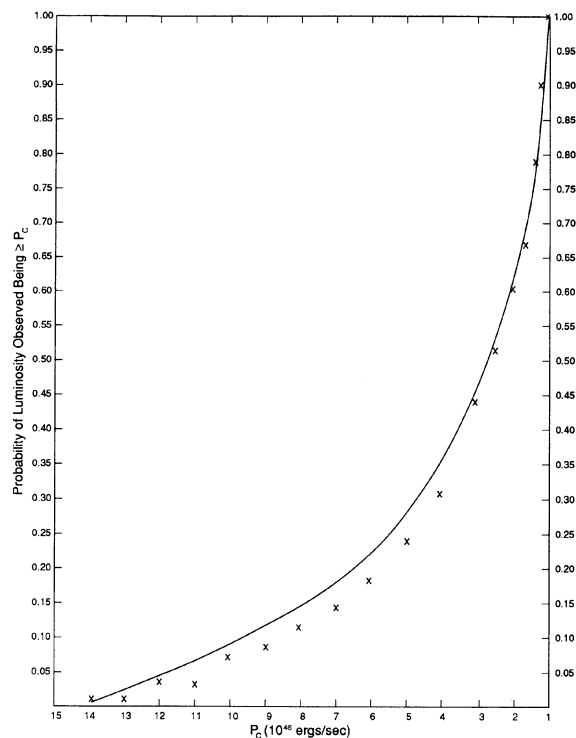


FIG. 1. A fit for the probability of a source exceeding or equaling P_c in observed luminosity for a standard beamed candle. The continuous curve is the theoretical partial distribution described in the text, $P(L)$. The crosses are the percent of the sample exceeding or equaling P_c in the catalog divided by 100.

lack of core-halo sources. In studies of flat spectrum cores, objects with halos have cores which are invariably too weak to make this survey (Antonucci & Ulvestad 1985 and Murphy *et al.* 1993). Also, there are only a handful of ultraluminous cores displaying diffuse emission comparable to the hot spot or jet. Much of this could be a consequence of the redshift dependence of the VLA to diffuse emission as a result of cosmological effects, the monochromatic surface brightness varies as $(1+z)^{-3}$ (Gunn 1978) and there is a factor of $(1+z)^{-\alpha}$, $\alpha=0.7$, for the K -correction. However, it is clear that no sources have strong diffuse emission in the context of FRII type luminosities. If diffuse emission is prominent, it is probably at best at the 3σ noise level. Thus, there is most likely no halo or diffuse emission above $3-4 \times 10^{44}$ erg/s in the sample of 134 [assuming the diffuse emission lies within 25 (arcsec) 2].

The main result of this paper is Table 1. 134 VLA targets were considered powerful enough to be included in the sample. Four other sources, marked with an asterisk were included which were observed only with the B-array at both 1.5 and 5 GHz (Feigelson & Isobe 1984). These naked cores were not ranked because they lacked sufficient resolution to see small scale jets, combined with the lower fluxes at 5 GHz compared to 1.5 GHz when $\alpha \approx 0.6$, for the jet emission. This is evidenced by 0938+119 and 0830+115 which were unresolved in Feigelson & Isobe (1984), yet the A-array observations of Neff & Hutchings (1990) at 5 GHz revealed

prominent small scale jets. The B-array observation do provide a limit on more extended emission which is useful to this study. The source 0805-046 was ranked since the B-array observation combined with the lower dynamic range A-array map at 5 GHz from Barthel *et al.* (1988) show the same amount of extended emission.

Column (1) of Table 1 gives the rank of the source in terms of P_c and Column (2) is the source name. Columns (3), (4), (5), and (6) tabulate P_c (in units of 10^{46} erg/s), P_E (in units of 10^{44} erg/s), $R=P_c/P_E$, and redshift, respectively. Column (7) gives the maximum Earth-based frequency, if less than 90 GHz, used to compute P_c . Columns (8) and (9) are the references for P_E and P_c , respectively. For naked cores the bound on P_E was chosen to be the 3σ noise level in an area on the order of 15 (arcsec) 2 at 1.5 GHz. At 5 GHz, it was based on the largest diffuse emission missed in a particular sample when compared to 1.5 GHz maps, and are signified with a question mark.

The most striking fact in Table 1 is the large range in R values. From 4.8 at the low end to at least 3580 (the sources with undetected extended emission might have even larger R values). This is not a matter of two sources with different core strengths, since the two most extreme cases have the same value of P_c to within 20%. These two sources are not freaks of nature either as there are other objects with similarly low and high R values. Clearly, there is a wide variety of physical circumstances occurring in the sample. It seems that there must be significant physics besides the angle to the line of sight of a relativistic beam to explain this.

It is worth commenting at this point on the effect of a different choice of H_0 and q_0 on the results of Table 1. Changing H_0 scales all luminosities equally independent of redshift. The choice of $q_0=0$, preferentially enhances intrinsic luminosities at high redshift. For instance if q_0 were taken to be 0.5, at $z=3$, the power would be 8/15 of the value in Table 1. This effect would shuffle the values of P_c in the table; however the top end of the luminosity distribution would still be dominated by high z sources even if $q_0=0.5$.

A scatter plot of P_c vs P_E is shown in Fig. 2 to help understand the statistics of Table 1. There are a few glaring features. First there are so many faint extended structures and nondetections. Between 42% and 47% have less than 10^{44} erg/s. For the sake of comparison, the extended emission in 3C 345 is 4.32×10^{44} erg/s and this is by no means a powerhouse in terms of extended emission. Secondly, the median is so small, less than 2×10^{44} erg/s or restated 3C 345 has more than twice the extended emission of over half the sources. To put this in perspective, the 3σ noise level for most of the sample extended over an $8'' \times 2''$ patch is larger than 10^{44} erg/s.

Thirdly, most of the sources are tightly clustered with P_E less than 5×10^{44} erg/s, and there is a gap in the scatter between 5×10^{44} erg/s and 7×10^{44} erg/s (probably a statistical coincidence). The sources with P_E larger than 10^{45} erg/s are clearly distinguished in this diagram. It is suggestive that there is some fundamental physics responsible for this. In the next section, we seek to answer why these sources have P_E values much larger than the rest of the sample.

4. THE HIGH END OF THE EXTENDED LUMINOSITY DISTRIBUTION

It is of interest to see what distinguishes the high end of the luminosity distribution for extended emission from the rest of the sample. In the following, it is argued that the extended emission is invariably dominated by a Doppler enhanced, relativistically beamed, kiloparsec scale jet in these sources.

In Sec. 4.1, the jet structures are analyzed through the available maps. It is argued that polarimetry data implies that the strongest knots in sources with large values of P_E are not hot spots, but part of the jetted beam. Also, there are many cases where maps show the terminal knot is much weaker than knots closer to the core. This information motivates the claim that the extended emission in most cases lies primarily in a jet, not a hot spot. Section 4.2 presents evidence for beaming in the kiloparsec scale jets and bounds the Doppler enhancement factor in each source. Section 4.3 analyzes the implications of this beaming analysis.

4.1. Jet Morphologies

Typically, the dynamic range is such that all of the extended emission which is detected resides in one or two knots. Often, a knot-like structure is only partially resolved from the core. The keys to interpreting the large sample of imperfect maps are provided by studying those sources which have been mapped with strong, well defined jets in situations when the maps were not ideal (i.e., only partially resolved and at low dynamic range), and extrapolating this insight to the more ambiguous maps in the sample. Detecting a jet is not a clear cut issue for core dominated sources within the framework of the beaming hypothesis, since they are viewed nearly end on. Thus, the criteria of the observed length being at least four times the width (Bridle 1984) is not necessarily true even for structures which are very elongated upon deprojection.

A distinction is usually made between the jet and terminal knot or hot spot. In steep spectrum, extended sources the hot spot is usually the brightest knot and the magnetic field in the hot spot is generally orthogonal to the jet direction (Garrington *et al.* 1991). To understand the nature of the hot spots in the kiloparsec scale jets of core dominated sources Table 2 was constructed. It tabulates the jet morphology of a subsample of sources with $P_E \geq 7.5 \times 10^{44}$ erg/s, for which more than one knot has been mapped. The table is derived from the maps in the Appendix and the quoted literature. The sources are arranged in order of extended power. Column (1) is the source name and Column (2) is the extended luminosity expressed in units of 10^{45} erg/s. Column (3) gives the number of knots and the frequency at which they were detected in parentheses. Those listings that are marked with asterisks were observed in polarized light which has higher resolving power since polarization is a vector which can change direction relatively quickly (on scales on the order of $0.1''$) along the jet. Consequently, in a few cases, more knots can be seen in the polarized maps than in a conventional map at the same frequency. Some of the knots are only partially resolved and their identification might be considered subjective.

The logic behind the knot identifications can be found in the notes for individual sources in the Appendix. The fourth column identifies the most luminous knot. Column (5) gives the percent of jet luminosity isolated in that knot and the direction of the magnetic field relative to the jet direction in parentheses, when available. Column (6) does the same for the terminal knot detected in the maps.

Of the thirteen sources in Table 2, the brightest knot is the terminal knot in only two cases. In one of these two cases, the magnetic field is parallel to the jet direction in the terminal knot. It is concluded that in twelve sources, the hot spot is not the most luminous knot. The one exception might be to 3C 454.3 for which no polarization data was found, surprisingly. In any event, by the asymmetry of the source, the radiative plasma in the terminal knot must be highly beamed. It seems very clear that the inner knots in these sources must be Doppler enhanced (this is quantified later in this section). In one instance, 0106+013, the terminal knot is almost 2 orders of magnitude weaker than the brightest knot. Thus, the terminal knot might not even be detected with the dynamic range in the available maps. The problem is exacerbated by needing high resolving power (5 GHz maps) to separate knots in a jet viewed nearly end on. If 3C 279 is any example, the hot spot in that source has a steeper spectrum than the rest of the jet and is harder to detect at high frequency (De Pater & Perley 1983; Perley *et al.* 1982).

The results of Table 2 are extrapolated in the following analysis as the basis for the critical assumption that any detection consisting of a single knot-like extended structure in the subsample, $P_E \geq 10^{45}$ erg/s, is considered to be jetted emission. Consistent with this is the small angular separations between the solitary knots and the core, less than $2.5''$ in all cases.

Table 3 presents the evidence of jet emission for all sources with $P_E \geq 7.5 \times 10^{44}$ erg/s. The maps for the subsample of interest, $P_E \geq 10^{45}$ erg/s, are analyzed in the notes for individual sources in the Appendix and are presented there as well, so that the readers can judge for themselves the validity of the entries in the table. There are four classes of extended structure referred to in Table 3.

Class I: The extended structure is clearly in jet form (at least 95% of the extended luminosity is in the jet).

Class II: Over 95% of the extended emission is in one secondary, unresolved structure which is disconnected from the core.

Class III: The extended structure is unresolvable from the core (core-extended) and manifests itself in the deformation of the core from the beam shape.

Class IV: There is more than 5% of the extended emission on the counterjet side.

Column (1) of Table 3 gives the rank in terms of extended luminosity. Column (5) gives the references for the maps. The angular size of the jet, θ_j , is displayed in Column (6). The percent of extended emission in the jet is listed in Column (7). Finally, Column (10) gives the classification of the extended structure. No maps were obtained for 0438-436 and 1032-199, only notes from Perley (1982). Unless there was polarization data to the contrary, all knots were considered part of the jetted emission.

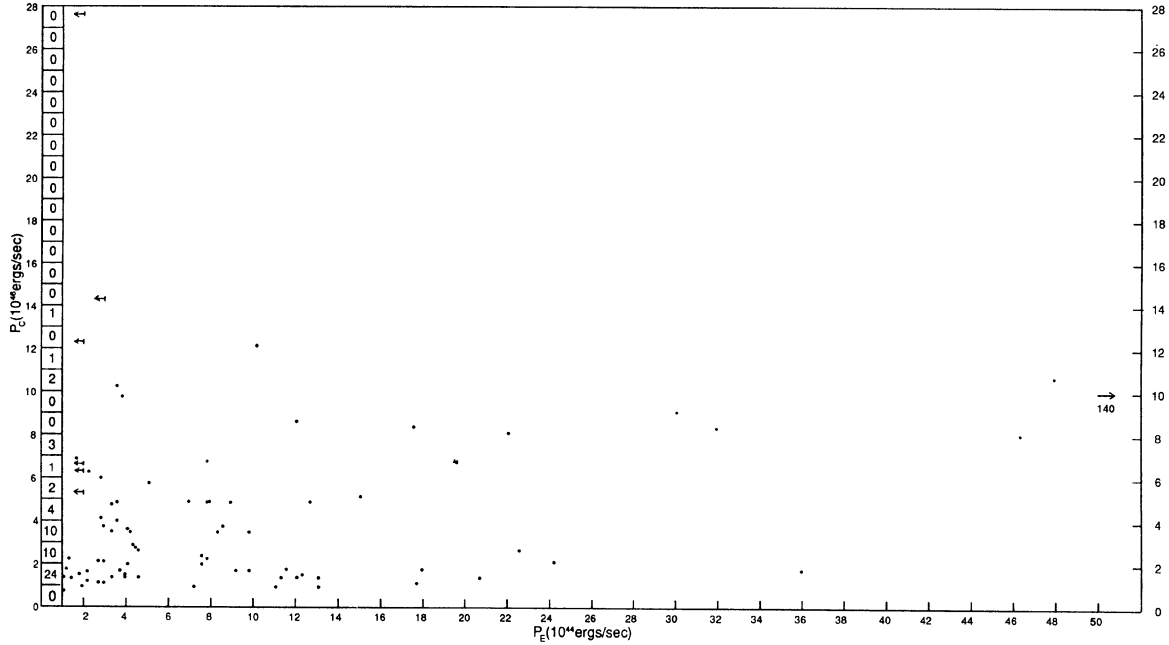


FIG. 2. A scatter plot of extended luminosity, P_E , vs core luminosity, P_C , for ultraluminous cores. Many sources are concentrated at $P_E < 10^{44}$ ergs/s. To represent this dense clustering of dots, the number of sources in “square” bins, 10^{46} ergs/s by 10^{44} ergs/s, are totaled inside of the squares. Sources with only upper limits above 10^{44} ergs/s on extended luminosity are indicated by arrows. The source 3C 446 has a value of $P_E = 140$ (in the units of the plot) and lies way off of the page, so it is indicated by an arrow.

By no means is Table 3 proof of jetted emission in all cases because of assumptions and extrapolations based on limited data. However, plausible arguments that the extended emission is dominated by Doppler enhanced, beamed energy can be made in all but two cases out of the subsample of 32 quasars with extended emission larger than 7.5×10^{44} erg/s (0229+132 and 2044–168 are probably exceptions). Whether the beamed jet interpretation is true for every source cannot be proved. However, it will be argued that the vast majority have strong emission as a result of Doppler beaming.

Over 90% of the subsample with $P_E \geq 10^{45}$ ergs/s have extended emission which is plausibly concentrated in a kiloparsec scale jet (Classes I, II, or III). To be certain of this fact, one would need high resolution, 8.5 GHz, images of the jets as well as polarization data. It would also be crucial to have 1.5 GHz high dynamic range data to help locate terminal knots or hotspots which seem to be faint for many of these sources.

4.2. Beaming of the Jets

There is evidence for jet beaming in the form of the asymmetry of the extended emission and its correlation with brightness in the subsample. Note the distribution of Class IV objects in Table 3 by rank: 10, 20, 24, 27, and 32. They clearly become more common as P_E decreases. This is consistent with relativistic beaming enhancing the brightness of the extended emission in the subsample of Table 3.

It is of interest to quantify this argument by placing a lower limit on δ , the Doppler enhancement factor, for each source. This would allow one to form an upper bound on the

intrinsic luminosity of the extended emission. The Doppler boosting enhances the luminosity by a factor δ^p , where

$$\delta = [\gamma - (\gamma^2 - 1)^{1/2} \cos \theta]^{-1}, \quad (1)$$

where γ is the bulk flow Lorentz factor, θ is the angle of jet propagation to the line of sight, and $p = 2 + \alpha$ or $3 + \alpha$ for a continuous jet or for spherical rest frame emission, respectively (Lind & Blandford 1985). Observationally, the Doppler effect is manifested by an asymmetry in jet luminosities on opposite sides of the core. Quantify this effect through the ratio of the two jet luminosities, J . Assuming bilateral symmetry

$$J = \left(\frac{1 + \beta \cos \theta}{1 - \beta \cos \theta} \right)^p. \quad (2)$$

To more accurately utilize Eq. (2), one should not compare the total emission on both sides of the core (such as filament, halo and hot spot emission), but only jet emission. This is made difficult by the fact that counterjets in quasars are very weak. In this subsample there are no counterjet detections. However, in a few cases, there is some detected emission on the counterjet side and conceivably some of it is in a jet which is unresolved from the rest of the lobe. The redshifts are high enough that the 3σ noise level can only limit the counter jet to $\lesssim 10^{44}$ ergs/s. This limit does not give a useful upperbound for J .

4.2.1 Bounding the counterjet luminosities

The maps do not have a large enough dynamic range to realistically bound J . To improve this bound, one can look at the most rigorous analysis of the faint counterjets of radio

TABLE 2. The knot structure of well resolved kiloparsec scale jets emanating from ultraluminous radio cores. The terminal knot which is observed is generally not very conspicuous. In the cases where polarimetry suggests that it is a "hot spot," it is often less prominent compared to the other knots in the jet as contrasted with the morphology of steep spectrum radio loud quasars. The columns are discussed in detail in the text.

Source	P_E (10^{46} ergs/sec)	# of knots (frequency)	Brightest Knot	% of Jet in Brightest Knot/ (θ)	% of Jet in Terminal Knot/ (θ)
0106+013	4.8	2(5 GHz) 8(8.5 GHz)*	6th	59%(II)	1.3%(I)
2037+511	4.65	2(5 GHz) 3(15 GHz)	2nd	65%(I)	20%(II)
0458-020	3.12	1(1.5 GHz) 2(5 GHz)	1st	40%	7%
1116+128	3.0	2(1.5 GHz) 1(5 GHz)	1st	95%(II)	5%
0805+046	2.4	3(5 GHz)	3rd	62%(II)	62%(II)
0149+335	2.25	2(1.5 GHz)	1st	80%	20%
1807+279	1.76	4(1.5 GHz) 5(5 GHz)	1st	50%	15%
0836+710	1.22	2(5 GHz)	1st	80%(I)	20%(II)
1020+191	1.15	2(5 GHz)	1st	60%	30%
1253-055	0.863	4(5 GHz)	1st	35%(II)	12%(I)
0119+247	0.789	3(1.5 GHz)	2nd	50%	25%
2251+183	0.783	4(1.5 GHz)	4th	90%	90%
1954+513	0.748	3(5 GHz)	2nd	50%(II)	5%(II)

loud quasars (Bridle *et al.* 1994). Their sample consists of steep spectrum 3C objects. According to the beaming hypothesis these objects lie closer to the sky plane than the core dominated objects considered here. Thus, it would not be appropriate to adopt these J values which should be larger in the core dominated sample. Table 4 tabulates some of the pertinent results of Bridle *et al.* (1994) necessary for bounding intrinsic counterjet luminosities.

Table 4 lists the ratio of lobe to jet flux at 5 GHz on the counterjet side in Column (2). The detected power in the counterjet, P_{cj} , is listed in Column (4) when it is not equal to zero. The object, 3C 68.1, has the most prominent counterjet candidate. Technically, no counterjet satisfies all of the properties necessary to be classified as a jet (Bridle 1993). However, this quasar probably lies very near the sky plane, within the context of the beaming hypothesis, since it is a red quasar and the radio core is extremely weak, 1 mJy at 5 GHz (Bridle 1993). The counterjet prominence relative to the lobe should increase with increasing θ from beaming considerations (assuming that the lobe emission is much less Doppler enhanced). Thus, based on Table 4, a conservative lower bound on the ratio of lobe to jet emission on the counterjet side of 25 is chosen for the core dominated sample. We proceed to make this bound even more conservative.

The strongest counterjet luminosities, P_{cj} , in the steep spectrum sample are 3C 68.1 and 3C 336 at 1.4×10^{43} ergs/s and 8.87×10^{42} ergs/s, respectively. As mentioned earlier, since 3C 68.1 is likely to lie much nearer to the sky plane than the more beamed, core dominated objects, an upper bound of 1.4×10^{43} ergs/s is probably too large for our subsample. In conclusion, the following conservative upper bound on the counterjet luminosity is chosen: The larger of 1/25 of the extended emission on the counterjet side or 10^{43} ergs/s which would be buried in the 3σ noise level in our maps.

4.2.2 Computing the Doppler enhancement

Table 5 tabulates the upper bounds on jet and source luminosities if the source were viewed in the sky plane, P_S , of

all sources with $P_E \geq 7.5 \times 10^{44}$ ergs/s based on the maps referenced in Table 3. Column (1) gives the ranking of the source in terms of extended emission. Column (2) is the source name. Column (3) gives a lower limit on J based on the bounds on counterjet luminosities conjectured in the previous paragraph and bilateral symmetry. Column (4) gives a bound on the largest probable angle to the line of sight, θ_{max} .

To find θ_{max} one needs to know something about the expected angular size of the source in the sky plane. Kapahi (1989) found that 3CR radio galaxies with $z > 0.8$ have a median angular size on the order of $25''$. Thus, a minimum angular size of $10''$ seems a conservative estimate. Any value larger than this will decrease the counter jet intrinsic power below our upper bound. It is true that if some of these objects are compact steep spectrum galaxies seen end on then $10''$ might be too large. In the spirit of the basic unified scheme it is assumed that the sources are FR II radio galaxies seen end on. Column (5) gives a minimum bulk flow Lorentz factor for the jet, γ_{min} , based on Columns (3) and (4) and Eq. (2). Column (6) gives a lower bound on the beaming factor, δ^P , in the jet. P is chosen to be 2.75 since it yields a smaller δ^P than 3.75. Column (7) is the corresponding upper bound on intrinsic jet luminosity, L_j . Column (8) is the upper bound on the luminosity of the jet if it were observed in the sky plane, L_S . Column (9) is the upper bound on observed emission from the counter jet, P_{cj} . Column (10) is the bound on the emission from a halo or counter lobe estimated from the morphology of the maps and the 3σ noise level, P_H . Finally, in Column (11), the luminosity of the source if it were viewed in the sky plane, P_S , is bounded. This allows a comparison of intrinsic strength with other steep spectrum objects. All powers in the table are expressed in units of 10^{44} ergs/s.

4.2.3 Notes on selected jets

Some notes on individual objects in Table 5 are given below.

0106+013: Another interpretation of the maps is that the two or three knots at the end of the jet combine to make up

TABLE 3. The morphology of the extended radio emission of ultraluminous radio cores with considerable extended luminosity. The extended structure is invariably dominated by a one sided kiloparsec scale jet. See the text for a description of the columns.

Rank	Source	P_E (10^{44} ergs/sec)	P_C (10^{46} ergs/sec)	Ref.	θ_j	% of Luminosity in Jet	R	z	Clas
1	2223-052	140	10	j,p	< 2"	100%	7.14	1.404	III
--	(3C446)	--	--	--	--	--	--	--	--
2	0106+013	48	10.6	a,f,g	5"	95%	22	2.107	I
3	2037+511	46.5	8.13	i	2.5"	> 95%	17.5	1.69	I
--	(3C418)	--	--	--	--	--	--	--	--
4	0119-046	35.9	1.72	d	2"	100%	4.8	1.95	II
5	0458-020	31.2	8.28	e,u,C	2"	95%	26	2.29	II
6	1116+128	30	9.02	a,i	5.5"	> 97%	30	2.118	I
7	0438-436	27.8	23.1	19	2.2"	~100%	83.1	2.85	II?
8	0805+046	24	2.02	h,w	4"	> 95%	8.4	2.877	I
9	0149+335	22.5	2.75	e	4"	> 95%	12.2	2.43	II
10	0229+132	22.0	8.03	a	4"	60%	36	2.065	IV
11	0830+115	20.7	1.30	e	4"	95%	6.3	2.97	I
12	0938+119	17.9	1.73	e	< 1"	100%	9.7	3.19	III
13	1807+279	17.6	1.23	d	5.5"	95%	7.0	1.76	I
14	2351-154	14.9	5.08	e	< 1"	100%	34	2.67	III
15	1624+416	12.7	4.70	i	0.7"	100%	37	2.55	III
16	0836+710	12.2	8.65	i	1.8"	100%	71	2.16	II
17	0812+332	12.2	1.01	e	< 1"	100%	8.3	2.42	III
18	2249+185	12.2	1.01	d	0.5"	100%	8.3	1.76	III
--	(3C454)	--	--	--	--	--	--	--	--
19	0258+058	12.2	1.55	e	1"	100%	2.7	2.31	II
20	0859+470	12.0	1.37	a,r	1.5"	> 80%	11.4	1.462	IV
21	1020+191	11.5	1.80	e	5"	100%	15.6	2.14	I
22	2126-158	10.2	12.2	e	2"	100%	120	3.27	II
23	1616+063	9.95	3.47	e	2"	100%	36	2.09	I
24	2044-168	9.7	1.72	d	10"	90%	17.8	1.937	IV
25	1551+130	9.01	1.58	e	1"	100%	17.5	2.21	II
26	1032-199	8.95	4.86	19	2.7"	100%	54	2.198	II?
27	1253-055	8.63	3.81	j,q	4.0"	> 80%	44	0.54	IV
--	(3C279)	--	--	--	--	--	--	--	--
28	0136+176	8.30	3.53	e	5"	100%	42.5	2.73	I
29	0119+247	7.89	2.33	e	10"	> 98%	30	2.03	I
30	2251+148	7.83	6.80	a	5.5"	~100%	86	0.859	I
--	(3C454.3)	--	--	--	--	--	--	--	--
31	0048-071	7.50	2.52	d	2"	100%	32	1.97	II
32	1954+513	7.48	2.01	f	12"	65%	27	1.23	IV

the hot spot instead of just the weaker terminal knot. If this is the case then the hot spot is probably beamed as well by considering the asymmetric extended structure. Since the hot spot is less elongated than the jet, $p=3.75$ is chosen (spherical emission in the plasma rest frame). One finds for the hot spot:

$$J > 34.3, \theta_{\max} < 20^\circ, p = 3.75, \gamma_{\min} = 1.13, \delta^p > 5.56,$$

$$L_i < 3.79 \times 10^{44} \text{ ergs/s}, \text{ and } L_S < 2.40 \times 10^{44} \text{ ergs/s}$$

and for the jet

$$J > 205, \theta_{\max} < 20^\circ, p = 2.75, \gamma_{\min} = 1.65, \delta^p > 11.17,$$

$$L_i < 1.84 \times 10^{44} \text{ ergs/s}, \text{ and } L_S < 4.77 \times 10^{43} \text{ ergs/s}.$$

Combining this information yields $P_S < 8.2 \times 10^{44}$ ergs/s.

1807+279: If the last knot is considered a hot spot, it would imply by an analogous calculation to that for 0106+013, above, that P_S could be as large as 5.5×10^{44} ergs/s.

3C 454: This is a compact steep spectrum source. Such sources are not considered beamed objects in a general sense (Fanti *et al.* 1990). More precisely this statement derives from statistical reasoning which shows that most are not beamed, however moderately beamed sources must sometimes get absorbed within the classification (Fanti *et al.* 1990). The one-sidedness of the extended emission suggests that this is the case here. If not, this source is different enough from the rest of the sample that it should not be included in this catalog.

2044-168: A very extended source, $35''$ long, which upon deprojection could be huge. It is unusual based on lobe advance speed arguments, in that the counter lobe is twice as far from the core as the jetted lobe. A very weak (3×10^{43} ergs/s), short jet points toward a strong knot $10''$ southeast of the core. This is so far from the core that it is considered a hot spot and the calculations in Table 5 were performed accordingly. This source lacks high frequency spectral data. It is this author's experience that for sources with this type of extended morphology that high frequency data will show a steep turnover rendering the core too weak for the catalog. Examples are 0850+518 (Garrington *et al.* 1991), 1508-055 (Hintzen *et al.* 1983; Ulvestaad 1993), and there is an extremely close resemblance to 1415+463 (Owen & Puschell 1984; Perley *et al.* 1982).

3C 279: This is a well studied object with a variety of extended structure. The breakdown of component luminosities are 7.0×10^{44} ergs/s in the jet, 9.66×10^{43} ergs/s in a steep spectrum hot spot and lobe which terminates the jet and 7.54×10^{43} ergs/s in the counter lobe.

4.3 Analysis and Conclusion

Table 5 reveals the importance of beaming for these sources. If all objects were to lie close to the sky plane then the Class IV objects would be the most luminous. The strongest source in the sky plane would be 0229+132 and it is quite different from the rest of the sample. It might be the only source with more than 5×10^{44} ergs/s in the sky plane

TABLE 4. The counterjet structure of a sample of steep spectrum quasars which were mapped with high resolution and very high dynamic range.

Source	Counter Lobe/Counter Jet 5 GHz Luminosity Ratio	z	P_{cj} (ergs/sec)
3C9	306	2.012	7.54×10^{42}
3C47	> 96	0.425	---
3C68.1	18.2	1.238	1.40×10^{43}
3C175	> 1,240	0.768	---
3C204	> 642	1.112	---
3C208	> 78.4	1.110	---
3C215	47	0.411	1.5×10^{42}
3C249.1	478	0.311	2.02×10^{42}
3C263	> 281	0.656	---
3C334	83.7	0.555	2.60×10^{42}
3C336	158	0.927	8.87×10^{42}
3C351	400	0.371	5.5×10^{40}
3C432	> 1,683	1.805	---

luminosity. Even if in the few debatable cases, one choses the knot furthest from the core which is detected to be a hot spot, none of the other sources should be close to 10^{45} ergs/s if viewed in the sky plane. Even such a conservative interpretation shows that the extended emission is not intrinsically strong, weak to moderate FR II luminosities at best. This effect is exaggerated by the fact that these sources are at high redshift ($z > 1.5$) for the most part. In this redshift range there is extended emission from some sources which is three orders of magnitude larger, for instance, 1318+133 (1.7×10^{47} ergs/s), 3C9 (7.5×10^{46} ergs/s) and 730+257 (6.2×10^{46} ergs/s) (Lonsdale & Barthel 1987). These particular sources were singled out since they have cores with on the order of 1 mJy of emission at 5 GHz, thus they are not seen face on and Doppler beaming should not be important, but technically can never be ruled out.

Doppler beaming has caused the strength of the extended

emission of core dominated objects to be overstated in the past. For instance, Antonucci & Ulvestaad (1985), emphasize that 3C 279 would make the 3C catalog based on extended emission alone. However, it is claimed here that if it lay near the sky plane (an FR II radio galaxy according to the beaming hypothesis) then its 178 MHz spectral flux would be less than 4 Jy. Out of the 138 objects in Table 1, only 3C 279 and a couple of other low z objects could make the 4C catalog if they were viewed near the sky plane and only a few more could make the 5C catalog.

Another fact that kiloparsec scale beaming explains is the large scatter in the high end of the extended luminosity distribution which is evident in Fig. 2. Looking at the upper bounds in Table 5, the extended intrinsic powers and especially the jet intrinsic powers look very homogeneous. It should be emphasized that even these jets are intrinsically weak for the redshift range in which they exist. If this beaming effect is prevalent for the other sources in the sample of 134, it might be that many of these other sources would have FRI luminosities if viewed near the sky plane (remember there are still many naked cores).

Another question which now becomes raised is why do some objects have these stronger jets? It is not because they are more along the line of sight than the rest of the sample, as evidenced by the number of jets larger than $2''$ in Table 3. The first thing to look at are correlations with P_c . However, as explained in Sec. 2, any such effect should be, and is, swamped by uncertainties and ambiguities in determining P_c . In the total sample, 17.2% of the objects have $P_E \geq 10^{45}$ ergs/s. However, 53% of the 17 most luminous cores have $P_E \geq 10^{45}$ ergs/s (see Table 1). Because of the scatter introduced in the determinations of P_c , when looking at the whole sample this effect can be masked statistically. This

TABLE 5. An analysis of Doppler enhancement in the kiloparsec scale jets emanating from ultraluminous radio cores. The results indicate that if these quasars were viewed near the sky plane then, in general, the extended luminosity, P_s , would appear quite weak. The columns are discussed at length in the text.

Rank	Source	J_{min}	θ_{max}	γ_{min}	δ_{min}^P	L_j	L_s	P_{cj}	P_H	P_s
1)	2223-052	1,400	9°	2.08	33.6	4.17	0.557	0.1	0.5	< 1.6
2)	0106+013	447	20°	1.93	14.48	3.08	0.505	0.128	3.07	2.57-4.07
3)	2037+511	465	15°	1.82	17.5	2.65	0.511	0.1	3.32	2.30-4.30
4)	0119-046	359	15°	1.74	15.73	2.28	0.497	0.1	1.0	0.7-2.7
5)	0458-020	312	9°	1.63	16.78	1.86	0.485	0.1	2.5	1.5-3.0
6)	1116+128	300	20°	1.76	13.05	2.30	0.513	0.1	1.8	0.8-2.8
8)	0805+046	240	20°	1.70	11.8	2.03	0.472	0.1	1.6	< 2.6
9)	0149+335	225	9°	1.55	14.33	1.57	0.470	0.1	1	< 2
10)	0229+132	37.1	15°	1.25	5.73	2.50	1.35	0.385	8.2	7.7-10.9
11)	0830+115	207	15°	1.58	12.58	1.64	0.466	0.1	1	< 2
12)	0938+119	179	6°	1.48	13.39	1.34	0.456	0.1	2	< 3
13)	1807+279	176	20°	1.61	10.41	1.69	0.456	0.1	1.9	0.9-2.9
14)	2351-154	149	6°	1.45	12.05	1.24	0.446	0.1	1	< 2
15)	1624+416	127	6°	1.42	11.05	1.15	0.438	0.1	1	< 2
16)	0836+710	122	6°	1.41	10.95	1.14	0.443	0.1	1	0.5-1.8
17)	0812+332	122	6°	1.41	10.95	1.14	0.443	0.1	1	< 2
18)	2249+185	122	6°	1.41	10.95	1.14	0.443	0.1	1	< 2
19)	0258+058	122	6°	1.41	10.95	1.14	0.443	0.1	1	< 2
20)	0859+470	67.2	6°	1.31	8.15	1.14	0.543	0.138	0.5	2.75-4.30
21)	1020+191	115	15°	1.44	9.78	1.18	0.433	0.1	1	< 2
22)	2126-158	102	9°	1.39	9.78	1.04	0.420	0.1	2	< 2.8
23)	1616+063	99.5	9°	1.39	9.61	1.04	0.420	0.1	1	< 2
24)	2044-168	8.9	30°?	1.06	2.80	3.18	2.56	0.1	2	5.0-7.0
25)	1551+130	90.1	6°	1.36	9.36	0.962	0.413	0.1	1	< 2
27)	1253-055	70	20°	1.38	7.40	0.946	0.40	0.1	2.22	1.72-3.32
28)	0136+176	83	20°	1.42	7.78	1.07	0.408	0.1	1	< 2
29)	0119+247	78.9	30°	1.55	5.87	1.34	0.40	0.1	1	< 2
30)	2251+148	78.3	20°	1.40	7.70	1.02	0.404	0.1	0.5	< 1.3
31)	0048-071	75	9°	1.34	8.35	0.90	0.402	0.1	1	< 2
32)	1954+513	74.8	30°	1.53	5.80	1.29	0.40	0.1	2.96	2.0-4.0

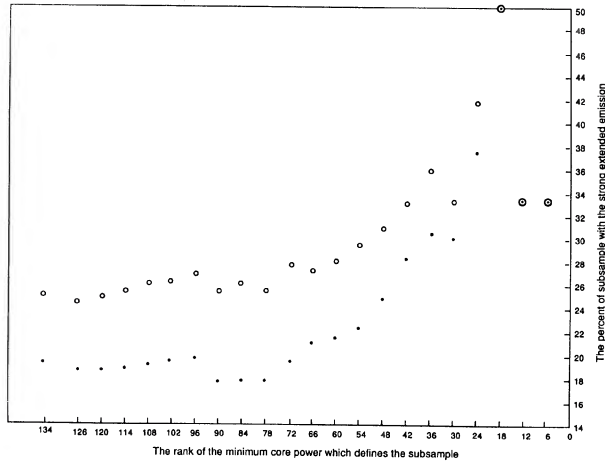


FIG. 3. The ultraluminous cores were ranked on the basis of core power in Table I. Subsamples were formed, defined by all the quasars with P_c ranking higher than a limiting rank. The percent of sources in these subsamples with strong extended emission is plotted vs the rank of the minimum core power defining the subsample. Circles represent sources with $P_E \geq 5.5 \times 10^{44}$ ergs/s and dots those sources with $P_E \geq 9 \times 10^{44}$ ergs/s.

effect is quite prominent if one looks at the frequency of strong extended emission as a function of subsamples defined by the rank of the minimum P_c in the population based on the rankings in Table 1. Figure 3 plots the percent of strong sources of P_E in a subsample, as a function of the number of sources in a subsample classified by minimum rank in core power. For example, the first point on the right of the horizontal axis is labeled “6”. This means that the six strongest cores are used as a subsample. The plotted point above this represents the percent of this subsample comprised of strong extended sources. A circle represents sources with $P_E > 5 \times 10^{44}$ ergs/s and a dot the percent of the subsample with $P_E > 9 \times 10^{44}$ ergs/s. The next point labeled “12” gives the percent of sources with strong P_E amongst the 12 strongest cores in Table 1 and so on. Figure 3 indicates that there is some correlation between the chance of P_E being large with P_c at the high end of the core luminosity distribution. However, statistically, the numbers are small so the strength of this correlation is not guessed at. For the rest of the sample no correlation between P_c and P_E is seen in the figure, as expected.

To see if the strong jets are an evolutionary phenomenon one can look at the correlations of P_E with z . This can be seen in Fig. 4 which looks at the frequency of strong extended emission as a function of ranked, redshift selected subsamples. This figure plots the percent of sources with strong P_E in redshift selected subsamples, where the horizontal axis labels the minimum rank of the z value in the subsample. For instance, a “60” on the horizontal axis means that the subsample consists of the 60 highest redshift sources out of 134 objects in Table 1. The points above “60” represent the percent of the subsample of 60 sources with strong extended emission. The circle and dot have the same meaning as for Fig. 3. The strong kiloparsec scale jets are most prominent when $1.7 < z < 3.0$. It should be noted that if the sample were binned by redshift subsamples ranked from

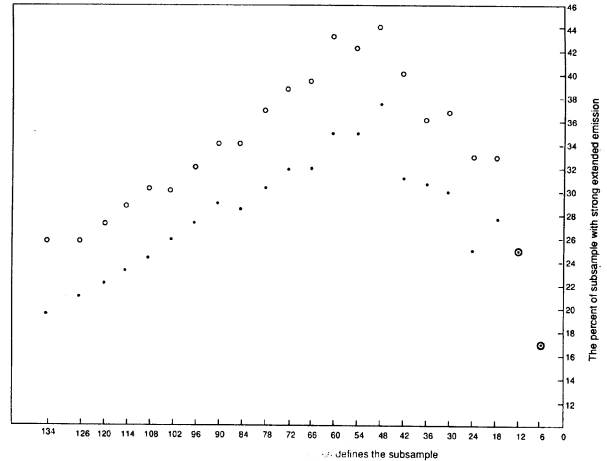


FIG. 4. The ultraluminous cores were ranked on the basis of redshift (highest to lowest). Subsamples were constructed, by defining all cores with redshifts ranking higher than a limiting rank. The percent of sources in these subsamples with strong extended emission is plotted versus the rank of the minimum redshift defining the subsample. The circles and dots have the same significance as in Fig. 3.

lowest instead of highest redshift, the same effect is seen. There are not enough high z ($z > 3$) sources in the catalog to be certain, but it appears that jet prominence begins to diminish at very high redshifts.

5. DISCUSSION

This article is an attempt to investigate the extended luminosity of intrinsically strong radio cores. It is argued through map morphologies and polarimetry data that the strongest extended emission is in the form of beamed kiloparsec scale jets near the line of sight. These jets had an epoch of prominence from about $z = 1.7$ to $z = 3.0$. If the objects in this sample were viewed near the sky plane, it is concluded from beaming calculations and from the number of naked cores that the vast majority of these quasars would have weak FRII luminosities at best. Since the 3σ noise level alone can mask very diffuse luminosities with FRII strength, it is difficult to assess just how weak the extended emission actually is. High dynamic range maps of sources suspected to have feeble extended luminosities, above 10 000, would help clarify the possibility of FRI level luminosities.

In any event, considering the high redshifts in the sample, these sources are quite weak. By comparison, if they were viewed near the sky plane, only 0229+132 would be luminous enough for the Barthel *et al.* (1988) sample of steep spectrum radio sources with $z > 1.5$. Even though extraordinary for this catalog, it would be one of the weakest sources in Barthel *et al.* (1988), ranking 81st or lower out of 90. In general, sky plane extended luminosities are three orders of magnitude weaker than the strongest steep spectrum quasars in the same redshift range. This implies two possibilities, either strong core power is anticorrelated with P_E , or the luminosity distribution for P_E is so steep that strong sources are extremely rare. The odds of seeing one being beamed towards us would even be smaller.

Another related issue is the lack of core halo objects in the sample which should be quite common according to the beaming hypothesis. There seems to be a paucity of diffuse lobe and halo emission in general. Perhaps this is only an artifact of limited dynamic range and the dependence of surface brightness on redshift.

This study suggests a few interesting observations. Many questions could be answered if one were to sit on a few of the objects with strong jets and no diffuse emission for many hours with the VLA at 1.5 GHz in both the A- and B-arrays. This was done in Antonucci (1986) for 3C 446 in the B-array with no luck. It would be interesting to know at just what level (if any) that the diffuse emission shows up. The best choices would be the lower z ($z < 2$) objects such as, 3C 446, 3C 418, 1807+279, 0859+470, and 0119-046, because of the $(1+z)^{-3-\alpha}$ dependence of the monochromatic surface brightness.

Another useful subsample to consider would be the naked cores. It might be worthwhile to get prolonged observations of cores which were already observed to be devoid of extended emission with high sensitivity by Murphy *et al.* (1993). If one were to choose those objects with $z < 2$ and sit on them for 5 or 6 hours at 1.5 GHz, one would have the best chance of finding a truly naked core.

I would like to thank Alan Bridle and Robert Antonucci for many enlightening discussions. I would also like to thank Chris O'Dea, Ron Kollgaard, Eric Feigelson, and Frank Briggs for permission to publish their maps. Special thanks to David Murphy and John Hutchings who freely shared their numerous map and knowledge.

APPENDIX

In this appendix the maps for the subsample $P_E \geq 10^{45}$ ergs/s are presented where possible. Based on these maps are notes for the individual sources. Table A1 lists the maps in the Appendix. The references are the same as those for Table 1. All maps were printed with the permission of the observers.

Notes on Individual Sources

The extended emission for all of the sources with $P_E \geq 10^{45}$ ergs/s is discussed in the context of the maps presented in this appendix. The sources are arranged in descending order of extended luminosity.

2223-052; 3C 446: The extended emission is extremely powerful compared to the rest of the sample and it is computed from early measurements of Brown *et al.* (1981) with the partially completed VLA. Contour maps of Fejes *et al.* (1992) at 5 and 1.6 GHz made with MERLIN indicate that the extended emission might be overestimated by almost a factor of 3 (it would still be the strongest extended source in the catalog). The emission is very compact, on the order of $1''$. Thus, it is unlikely that the 1.6 GHz MERLIN map could have missed 2 Jy with its $0.2''$ resolution in such a small region. The 408 MHz map of Browne *et al.* (1982) reveals only 0.25 Jy between $1''$ and $2''$. The compact nature of this

source is highlighted by Antonucci (1986) who detected no extended emission at 1.5 GHz in the B-array ($4.4''$ resolution) achieving a dynamic range of 5000!

The compact structure is extremely complicated and since no VLA A-array map at 5 GHz is available, it is presumed that any emission on scales larger than $0.2''$ could be detected as deformations of the core if observed with the VLA. This follows from other maps in this sample, see 1624+416 for example. Most of this emission would be missed at 1.6 GHz in the A-array. This source shows the imperfections of our core definition. At 1.6 GHz this might appear to be mostly an unresolved steep spectrum core with a very bright flat spectrum source embedded inside [this is a special case of a CSS core as suggested in Fejes *et al.* (1992)].

The jet structure is very twisted and is by no means well determined from the available maps. From VLBI maps of Simon *et al.* 1985 and Fejes *et al.* (1992) as well as the MERLIN 5 GHz map in the latter reference, it is clear that a strong jet emerges from the core slightly south of east for about 450 mas. Then, within 50 mas, becomes slightly west of north! On the 5 and 1.6 GHz map with MERLIN, there is also strong emission 100 mas north of the core. Is this another jet in the same quadrant? I believe it is not, but high frequency polarization data and deep high resolution maps are needed to determine this. If both are jets this would be hard to reconcile with the beaming hypothesis. All of the emission might be part of a single twisted jet with the emission north of the core a strong knot. The key evidence are the fourth and especially the fifth lowest contours in the 1.6 GHz map. Consider the 200 mas resolution of the map; if these were two distinct jets then these contours between the jets should have negative curvature, as does the sixth and seventh contours. In the 5 GHz map, one sees the emission become very weak as it turns 90° at the end of the east directed jet (perhaps moving away from the line of sight). The fourth and fifth contours on the 1.6 GHz map are consistent with this jet continuing to curve, but being relatively weak. As it hits the strong knot it is moving nearly due west (a 180° turn!). These maps as well as the 408 MHz map indicate that the jet might turn towards the northwest for about $1''$ after this, but it is very weak. Remember, that this twisting is greatly exaggerated by projection effects for a jet seen end on; it can be a manifestation of small wiggles.

In summary, the jet structure in 4C 446 appears to be very twisted and very close to the line of sight. However, more observations are needed to understand this very complicated source. Other examples of quasars with kiloparsec scale jets which turn 180° exist such as 0814+425 from Murphy *et al.* (1993). It is not as tightly coiled as 3C 446, but just as twisted, so it is easier to trace the jet.

0106+013: (Figs. A3 and A4) This is an important object for the rest of the study since a variety of maps and resolutions exist. The map in Fig. A4 is from the study of core dominated objects in Kollgaard *et al.* (1990). It has the strongest extended emission in that study by a large margin and it is the only object where it is concentrated in the jet (no halo emission). Kollgaard *et al.* (1994) have produced a variety of superior maps since then which will be described in the following. The strong jet points due south and radiates

TABLE A1. A description of the observing parameters used to generate the maps in the Appendix. The references are coded as for Table 1.

Figure	Source	Frequency (GHz)	Array	Reference
A1	2223-052	5	MERLIN	B
A2	2223-052	1.6	MERLIN	B
A3	0106+013	5	A	f
A4	0106+013	1.6	A, B, C	a
A5	2037+511	5	A	i
A6	2037+511	15	A	i
A7	0458-020	0.408	MERLIN	C
A8	0458-020	5	MERLIN	C
A9	1116+128	5	A	i
A10	1116+128	1.6	A, B, C	a
A11	0805+046	5	B	h
A12	0229+132	1.6	A, B, C	a
A13	1624+416	5	A	i
A14	0836+710	5	A	i
A15	0836+710	1.6	A, B, C	a
A16	0859+470	1.6	A, B, C	a

4.55×10^{45} ergs/s. On the counter-jet side there is 2.5×10^{44} ergs/s of luminosity. At 8.5 GHz, eight knots can be seen in the jet in polarized light. In unpolarized light at 5 and 8.5 GHz the final three knots appear as one due to insufficient resolution and the very intense luminosity of the first knot in this cluster (4.45" from the core). This bright knot is the only one visible in Fig. A4 which is not as deep as the more recent maps. The existence of the second knot (4.8" from the core) is clear in polarized light at both 5 and 8.5 GHz, but it is undetectable in the total intensity images. The third knot (5" from the core) is more debatable because it is defined by only the two lowest contours at 8.5 GHz in the polarized image. Consistently, a similar feature exists in the 5 GHz polarized image and even the 5 GHz total intensity map. In this scenario, the jet appears to veer due east in the last 0.5". This structure reveals a classical jet magnetic field configuration. At 8.5 GHz, the magnetic field is parallel to the jet direction through the first two knots in the cluster, then becomes perpendicular to the jet in the third knot after the jet has turned eastward. Thus, the knot 5" from the core could be considered a hot spot. A similar curved structure is seen near the end of other jets in Table 3 in such objects as 0836+710 and 1954+513. It should be noted that if the cluster of knots were viewed near the sky plane then the knots would most likely have an angular separation on the order of 2". Another interpretation has been suggested by Bridle (1993) that the second knot is probably a hot spot and the third knot is actually just part of the lobe emission, but one would need higher resolution to be sure. In either interpretation, the first knot in the cluster is much more luminous than the hot spot.

Another interpretation would be to call the whole structure a hot spot. In support of decomposing the structure, the asymmetry in hot spot luminosities, between the jet and counter jet sides, would be inconsistent with the relatively slow advance speeds (0.2c–0.3c) commonly associated with hot spots (Browne & Perley 1986). If a faster flow through the hot spot is responsible for the emission then this is equivalent to considering the emission at the hot spot as part of the jet for our beaming analysis.

The 1.6 GHz map of Murphy *et al.* (1993) in Fig. 8 is of

lower resolution and is a good example of what one would expect to see in the under-resolved images prevalent in the rest of the sample when a jet is present.

2037+511, 3C 418: (Figs. A5 and A6) O'Dea *et al.* 1988 have published excellent maps of this source at 5 and 15 GHz. There are three clear knots at 15 GHz, but at 5 GHz the second and third knots are only partially resolved from each other. The magnetic field is parallel to the jet direction in the outermost knot. The second knot has the magnetic field perpendicular to the jet direction. It is concluded that this structure is the jet and does not include a hot spot (i.e., the whole structure is the jetted beam). Again, virtually all of the extended emission is in the jet.

0119–046: This has been mapped by Barthel *et al.* (1988) and Neff *et al.* (1989) at 5 GHz. Both show a single secondary structure to the east, about 2" from the core. The map of Neff *et al.* (1989), at higher dynamic range, shows a faint bridge almost connecting the two components. This looks similar to the under-resolved image of 0106+013 at 1.6 GHz, suggesting that the extended structure is a bright knot in a jet. The evidence that it is part of the jetted beam and not a hot spot is only circumstantial, based on the results of Table 2. The core power is not well known, since there is no spectral information above 5 GHz. It is possible that this is not an ultraluminous core. Again, it is concluded that the detected extended emission is in the jet.

0458–020: (Figs. A7 and A8) Neff & Hutchings (1990) have a map at 5 GHz with a secondary structure to the southwest about 2" from the core. There is a bridge-like structure almost connecting it with the core. The secondary appears to be a partially resolved image of a double knot, with the luminosity concentrated in the inner-most knot. The structure is clarified by the MERLIN maps at 5 GHz and 408 MHz of Briggs *et al.* (unpublished). The 408 MHz map clearly shows the jet and the second knot are part of a very twisted jet. There is also some lobe luminosity on the counterjet side as well as some halo emission on the jet side. It is unclear if the second knot is a hot spot or the jet bends 90° to the east afterward. The 5 GHz MERLIN map shows that about half of the extended emission in the Neff & Hutchings (1990) is a straight jet propagating due west of the core between 0.1" and 0.5" (the contours are bunched together on the VLA map). It is concluded that the strong knot and 0.5" straight jet are definitely part of the jetted beam, implying the extended emission is jet dominated.

1116+128: (Figs. A9 and A10) O'Dea *et al.* (1988) show a map at 5 GHz with the core elongated towards a strong knot 2" from the core. The magnetic field is aligned with the jet direction. A second, much fainter, knot 5" from the core is seen at 1.6 GHz by Murphy *et al.* (1993). Thus, most of the extended emission is in the jet not the hot spot.

0438–436: No map is available, only the notation of a single secondary 2.2" away from the core reported by Perly (1982). It is conjectured that this is a strong knot in a jet.

0805+046: (Fig. A11) This has been observed by Barthel *et al.* (1988) at 5 GHz in the A-array with 0.5" resolution and by Feigelson *et al.* (1984) at 1.5 and 5 GHz (resolution of 1.3") in the B-array. The higher resolution map of Barthel *et al.* (1988) shows three distinct knots all of which lie

within the partially resolved jet shown in the 5 GHz map of Feigelson *et al.* (1984). Feigelson *et al.* (1984) shows that the magnetic field is aligned with the jet along its entire length. This is only apparent when one realizes that the jet veers toward the west near the end, which is very clear in the A-array map. Again, the extended emission lies in the jetted beam. There might be some emission on the counter jet side, in the lowest contour at 5 GHz as suggested by the 1.5 GHz map in the B-array. Its luminosity would be slightly less than 10^{44} ergs/s. The power of the core is not well known since there is no spectral information above 8.1 GHz. It is remotely possible that this is not an ultraluminous core.

0149+335: This object is mapped in Neff & Hutchings (1990) at 1.5 GHz. A secondary structure 2" away from the core is connected by a bridge, suggesting that the secondary is an unresolved cluster of knots in a jet. It appears that the jet flows to the northwest then bends abruptly in a strong knot towards the east for another 1.5"–2". The second leg of the jet may only be one knot, however it is much weaker than the first. Thus, most of the energy radiated is from the jet and not the hot spot. It is conjectured that the detected emission resides in a curved jet.

0229+132: (Fig. A12) This is the most unusual object in the subsample. It is the only object which displays considerable emission on both sides of the core. Unfortunately, the map at 1.6 GHz by Murphy *et al.* (1993) does not have sufficient resolution. Thus, it is impossible to tell if there are two jets or the more logical possibility that one side is a partially resolved hot spot and the other side is a partially resolved jet. David Murphy (1993) has indicated that the emission to the southwest is the more plausible candidate for a jet.

0830+115: This was mapped at 1.5 GHz by Neff & Hutchings (1990). Thus, the resolution is unable to isolate individual knots. The extended structure on the largest scales is elongated to the north by northeast. Looking at the core region it looks slightly elongated to the northeast on scales less than an arc second. This suggests a mildly curving, under-resolved jet is where most of the extended emission resides. Clearly, the resolution is not good enough to know this with complete certainty. Barthel *et al.* (1988) identified this as an unresolved core. There is no spectral data point above 5 GHz, so it is possible that this is not an ultraluminous core.

0938+119: This is a good example of a core-extended object in the 1.5 GHz map of Neff & Hutchings (1990). The source is unresolved in Barthel *et al.* (1988). The extended emission lies to the northeast within 1" of the core. This type of structure is considered to be the same as that of 0119–046, except the secondary is so close to the core that it is only partially resolved. It is conjectured that the extended emission is a jet seen nearly end on. No spectral data points exist above 5 GHz, so it is possible that this is not an ultraluminous core.

1807+279: Excellent maps of this source were made by Neff *et al.* (1989). The extended emission is clearly dominated by a jet. It is conceivable that the outermost knot is a hot spot, but it still contains less than 1/4 of the total jet luminosity.

2351–154: This is a deformed core, elongated to the northeast in the 1.6 GHz map of Neff & Hutchings (1990). This is interpreted as being due to a jet seen nearly end on. The flux in the jet is hard to estimate and it might be a little on the high side.

1624+416: (Fig. A13) A high resolution map at 5 GHz by O'Dea *et al.* (1988) shows an extension north by northwest of the core about 0.5" long. This emission was missed in the lower resolution map of Murphy *et al.* (1993) at 1.6 GHz. The magnetic field is parallel to the jet direction along its length, so the emission is probably not concentrated in a hot spot. Again, it is concluded that the extended structure is confined to a jet seen nearly end on.

0836+710: (Figs. A14 and A15) A high resolution, 5 GHz map can be found in O'Dea *et al.* (1988). The map of Murphy *et al.* (1993) only partially resolves the extended structure from the core, since the resolution is 1.3". At 5 GHz, a secondary exists 1"–1.5" from the core. It is in line with the VLBI jet detected by Pearson & Readhead (1988). The secondary appears to be a partially resolved cluster of knots. The innermost knot is the brightest, lying southwest of the core. The jet appears to veer to nearly due west after this knot with the magnetic field parallel to the jet direction at the terminus of the second knot. It is concluded that all of the detected emission at 5 GHz is in the jetted beam. The only emission on the counter-jet side at 1.6 GHz is at the same level as the negative contours.

0812+332: A map at 1.5 GHz was obtained by Neff & Hutchings (1990). The core is extended about 1" to the southwest. It is conjectured that the extended emission is concentrated in a jet seen nearly end on. There is no spectral data point above 5 GHz, so this might not be an ultraluminous core.

2249+185, 3C 454: This has a strong steep spectrum core which has been mapped in Barthel *et al.* (1988) and in Neff *et al.* (1989) at 5 GHz. It has an elongation of the core to the northwest, about 0.5" long. This is interpreted as a jet. There are quite a few high redshift compact steep spectrum objects in Barthel *et al.* (1988) with a similar morphology.

0258+058: A map at 5 GHz by Neff & Hutchings (1990) shows a distinct series of weak "knots" directed 10" to the west of the core. This is probably noise (Hutchings 1993). There is a strong knot 1.0" from the core that is not colinear with the other pseudo-knots. This extended emission is considered a jet pointing slightly southwest, but seen nearly end on. The map is noisy and the flux might be overestimated in Neff & Hutchings (1990). Again, it is concluded that the extended emission is concentrated in a jet. There are no spectral data points above 5 GHz, casting some doubt as to whether it is an ultraluminous core.

0859+470: (Fig. A16) There is a low dynamic range, high resolution, 5 GHz map by Perley *et al.* (1980) and a high dynamic range, low resolution, 1.6 GHz map by Murphy *et al.* (1993). The extended emission is dominated by an extension to the northwest less than 2" long, which is much easier to discern in the 5 GHz map. This is considered an unresolved jet. The 1.6 GHz map shows some diffuse emission on the counter-jet side within 3" of the core.

1020+191: This was mapped at both 1.6 and 5 GHz in Neff & Hutchings (1990). The extended emission is a jet pointing to the northeast. There is no spectral data point above 5 GHz, leaving the core luminosity in some doubt.

2126-158: A map at 1.5 GHz was created by Neff & Hutchings (1990) for this high redshift source. A faint unre-

solved secondary is seen about 1.5" from the core. It is interpreted as a bright knot in a jet.

1616+063: The 5 GHz map of Neff & Hutchings (1990) shows a short 2" jet pointing to the southwest with only one knot. It is concluded that the detected emission is in a jetted beam.

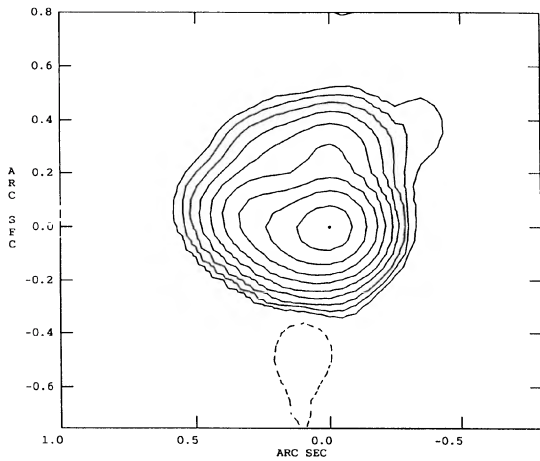


FIG. A1. A very high resolution map of 2223-052 showing a strong jet and complicated structure.

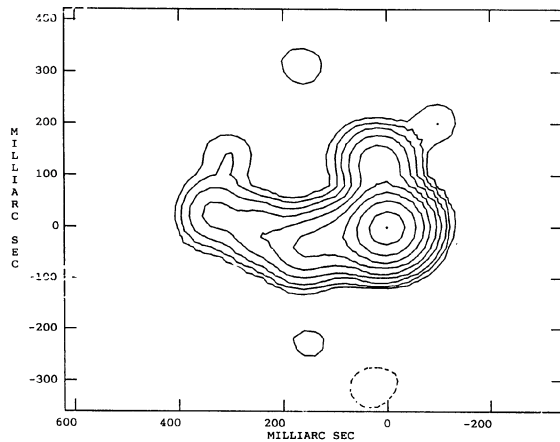


FIG. A2. Slightly less resolution and higher dynamic range than Fig. A1 reveals more clues to the extended structure of 2223-052.

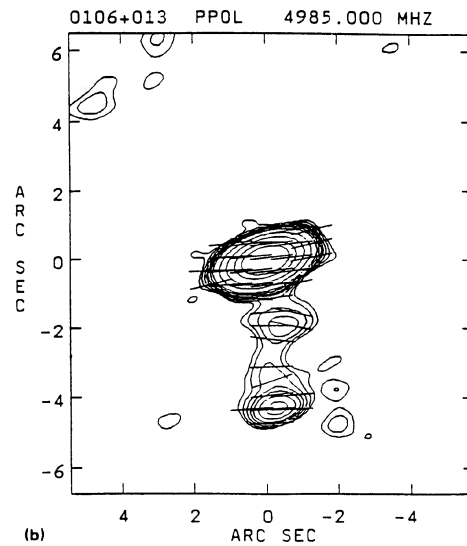


FIG. A3. A high resolution map of 0106+013, showing a strong jet.

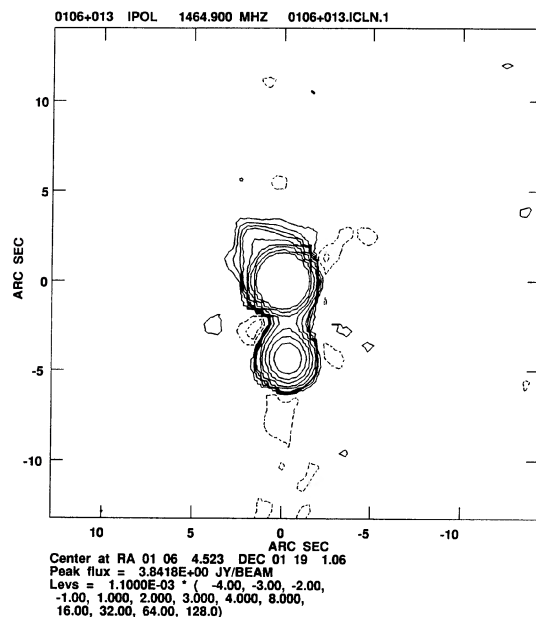


FIG. A4. A low resolution, very high dynamic range map of 0106+013.

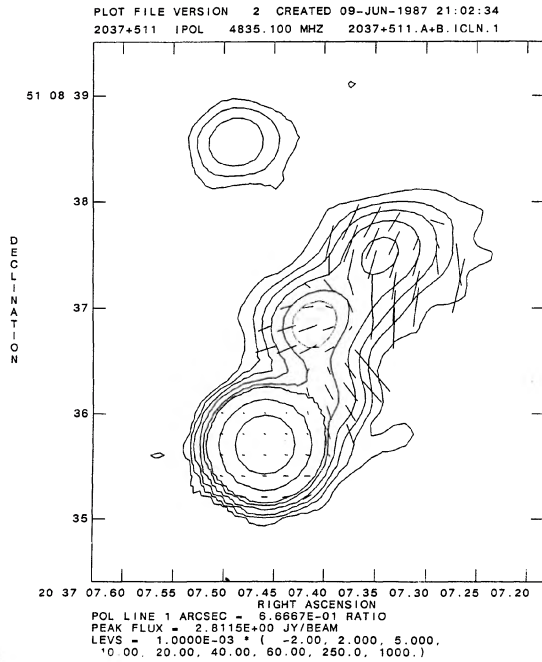


FIG. A5. A high resolution map of 2037+511.

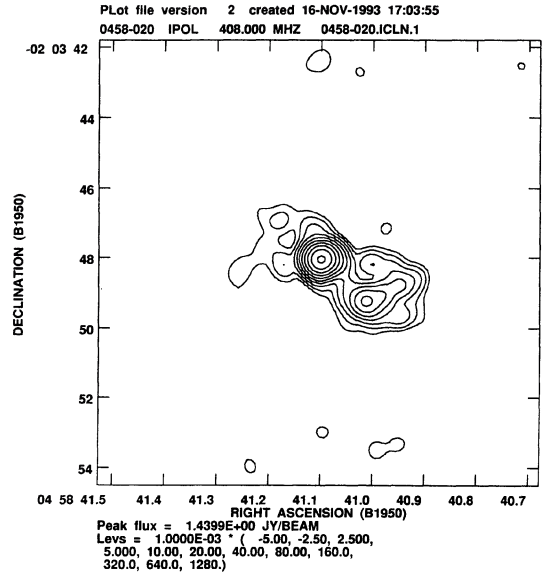


FIG. A7. Low resolution map of 0458-020 reveals the extended structure.

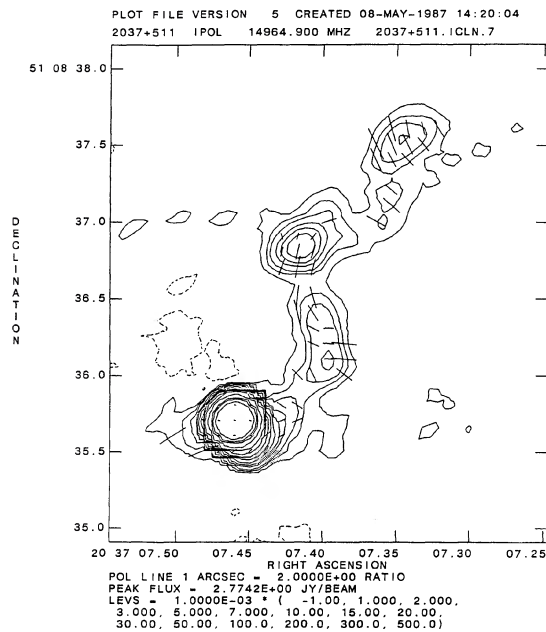


FIG. A6. A very high resolution map showing the jet structure of 2037+511.

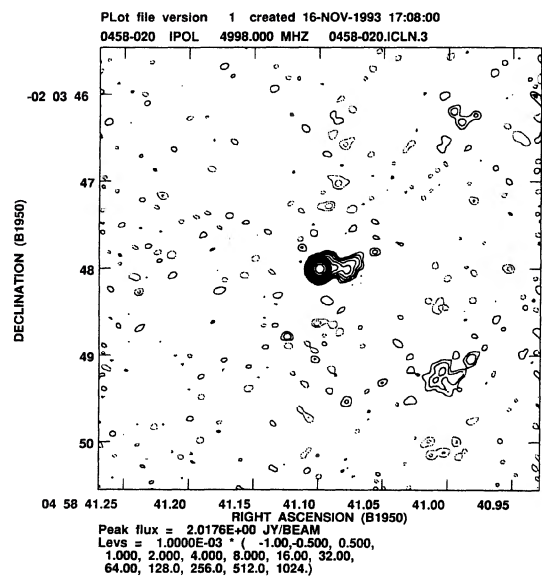


FIG. A8. This very high resolution image of 0458-020 shows the inner structure of the jet.

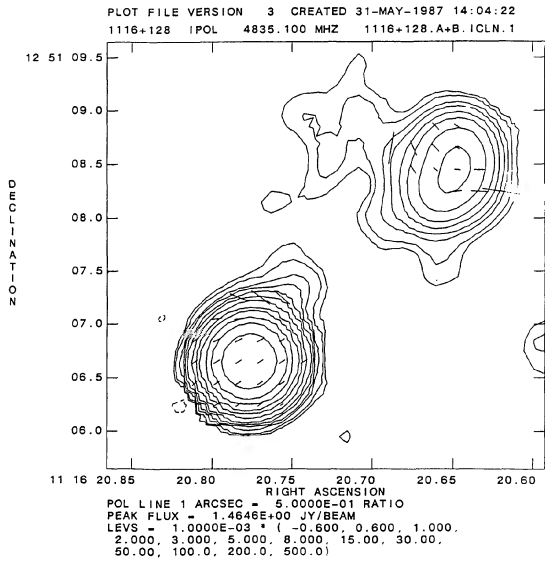


FIG. A9. High resolution image of 1116+128.

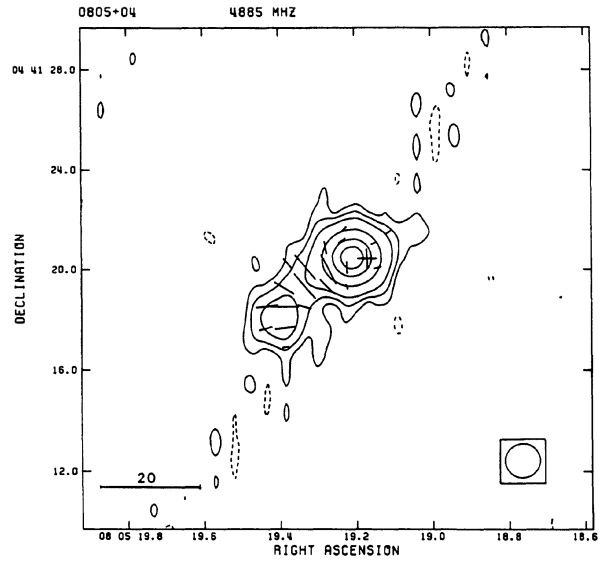


FIG. A11. Low resolution, low dynamic range image of 0805+046 which makes it hard to estimate the amount of extended emission on the counterjet side accurately.

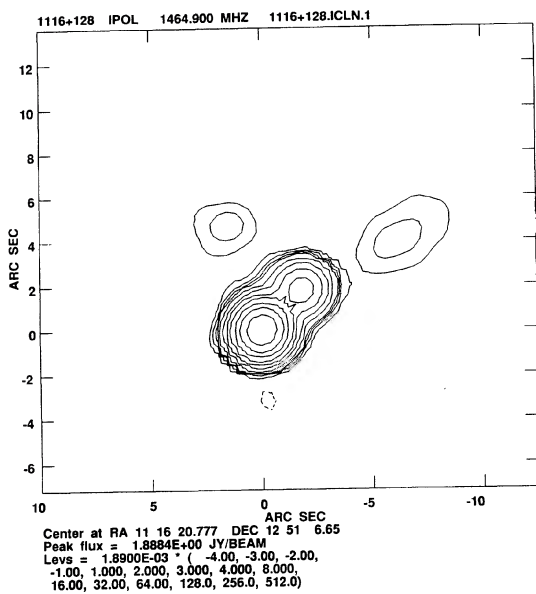


FIG. A10. Large dynamic range reveals more extended structure in 1116+128.

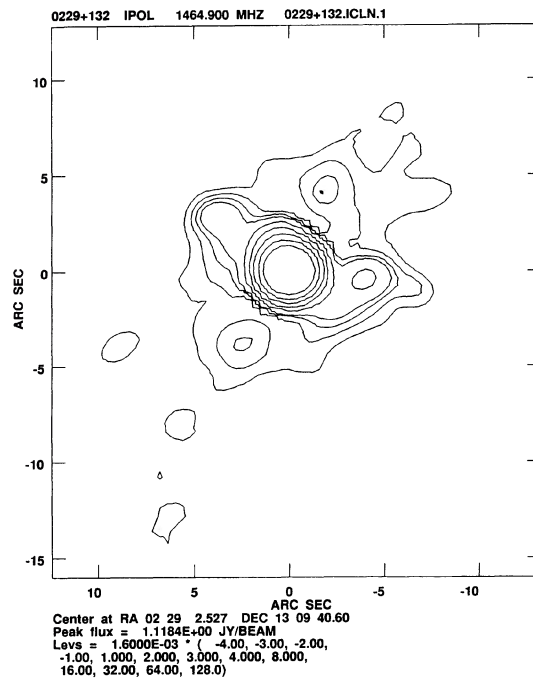


FIG. A12. Low resolution, high dynamic range map of the exceptional object 0229+132.

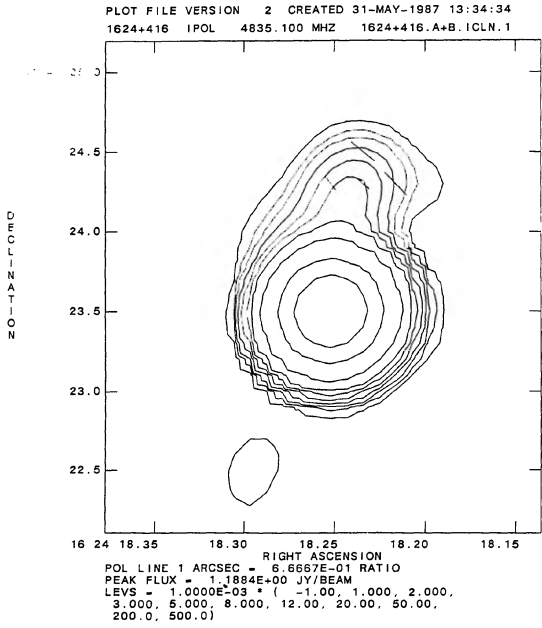


FIG. A13. High resolution image of 1624+416.

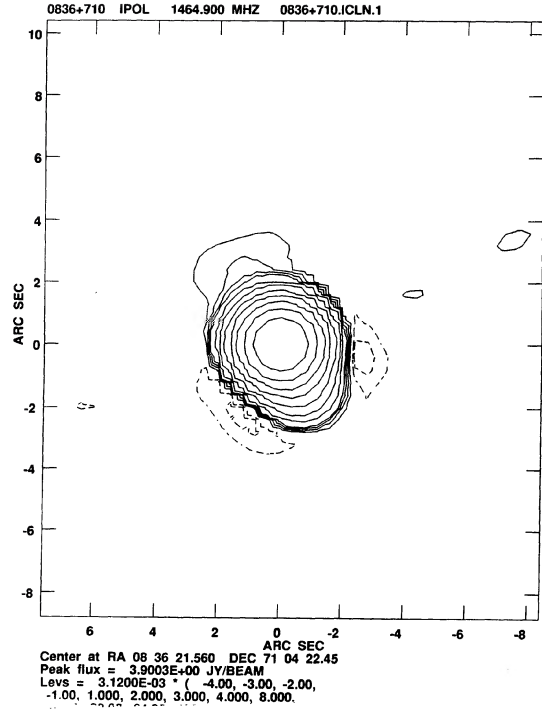


FIG. A15. The large dynamic range in this map of 0836+710 does not reveal any more extended structure.

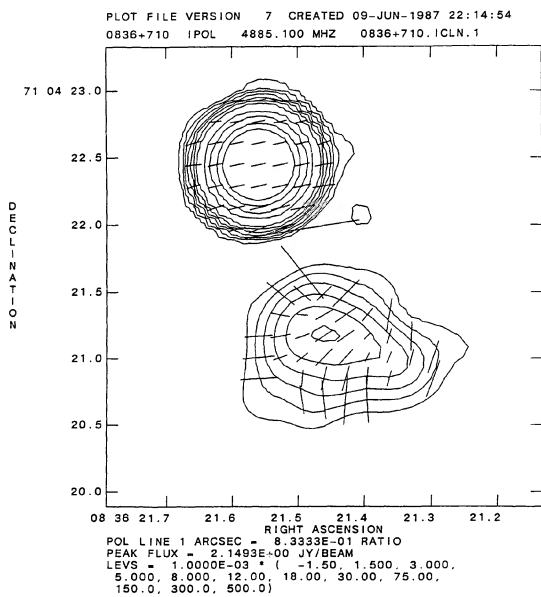


FIG. A14. High resolution map of 0836+710.

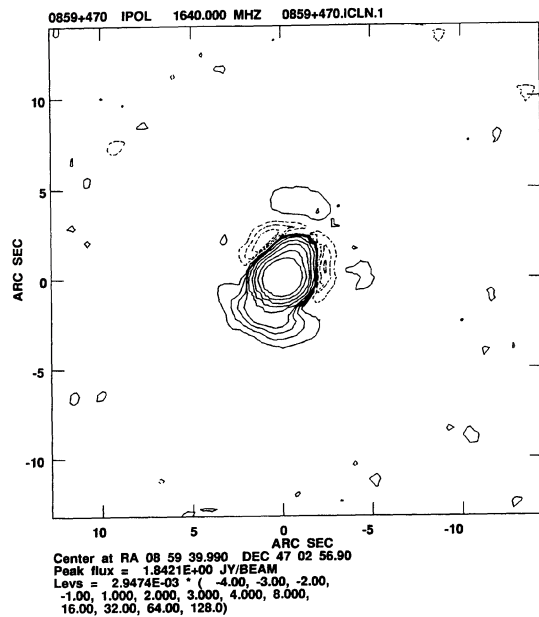


FIG. A16. A high dynamic range map of 0859+470.

REFERENCES

- Abraham, Z., De Medeiros, J. R., & Kaufmann, P. 1984, *AJ*, 89, 200
- Antonucci, R. R. J. 1993, *ARA&A*, 31, 473
- Antonucci, R. R. J. 1986, *ApJ*, 304, 634
- Antonucci, R. R. J., Hickson, P., Olszewski, E. W., & Miller, J. S. 1986, *AJ*, 92, 1
- Antonucci, R. R. J., & Ulvestad, J. S. 1985, *ApJ* 294, 158
- Barthel, P. D. 1989, *ApJ*, 336, 606
- Barthel, P. D., Miley, G. K., Schilizzi, R. T., & Lonsdale, C. J. 1988, *A&AS*, 73, 515
- Blandford, R. D., & Konigal, A. 1979, *ApJ*, 232, 34
- Bridle, A. 1984, *AJ*, 89, 979
- Bridle, A. 1993, private communication
- Bridle, A., Hough, D., Lonsdale, C., Burns, J., & Laing, R. 1994 (unpublished)
- Bridle, A., & Perley, R. 1984, *ARA&A*, 22, 319
- Briggs, F. H., Wolfe, A. M., Liszt, H. S., Davis, M. M., & Turner, K. L. 1989, *ApJ*, 341, 650
- Brown, R. L., Johnston, K. L., Briggs, F. H., Wolfe, A. M., Neff, S. G., & Walker, R. C. 1981, *ApJ*, 21, L105
- Browne, I. W. A., Clark, R. R., Moore, P. K., Muxlow, T. W. B., Wilkinson, P. N., Cohen, M. H., & Porcas, R. W. 1982, *Nature*, 299, 788
- Browne, I. W. A., & Murphy, D. W. (1987), *MNRAS*, 226, 601
- Browne, I. W. A., & Perley, R. A. (1986), *MNRAS*, 222, 149
- Chini, R., Biermann, P. L., Kreysa, E., & Gemünd, H.-P. 1989, *A&A*, 221, L3
- Chini, R., Steppe, H., Kreysa, E., Krichbaum, Th., Quirrenbach, A., Schalinski, C., & Witzel, A. 1988, *A&A*, 192, L1
- Conway, J. E., & Murphy, D. W. 1993, *ApJ*, 411, 89
- De Pater, I., & Perley, R. 1983, *ApJ*, 273, 64
- Edelson, R. A. 1987, *AJ*, 94, 1150
- Fanti, R., Fanti, C., Schilizzi, R. T., Spencer, R. E., Rendong, N., Parma, P., van Bruegel, W. J. M., & Venturi, T. 1990, *A&A*, 231, 333
- Feigelson, E., & Isobe, T. 1984, *AJ*, 89, 1464
- Fejes, I., Porcas, R. W., & Akujor, C. E., 1992, *A&A*, 257, 459
- Garrington, S. T., Conway, R. G., & Leahy, J. P. 1991, *MNRAS*, 250, 171
- Geldzahler, B. J., & Witzel, A. 1981, *AJ*, 86, 1306
- Geldzahler, B. J., & Kühn, H. 1983, *AJ*, 88, 1126
- Ghisellini, G., Padovani, P., Celotti, A., & Maraschi, L. 1993, *ApJ*, 407, 65
- Gunn, J. E. 1978, in *Observational Cosmology*, 8th Advanced Course Swiss Society of Astronomy and Astrophysics, edited by A. Maeder *et al.* (Geneva Observatory, Switzerland)
- Hintzen, P., Ulvestad, J., & Owen, F. 1983, *AJ*, 88, 709
- Hutchings, J. B. 1993, private communication
- Hutchings, J. B., Price, R., & Gower, A. 1988, *ApJ*, 329, 122
- Kapahi, V. K. 1989, *ApJ*, 97, 1
- Kellermann, K. I., Pauliny-Toth, I. I. K., & Williams, P. J. S. 1969, *ApJ*, 157, 1
- Kollgaard, R. I., Wardle, J. F. C., & Roberts, D. H. 1989, *AJ*, 97, 1550
- Kollgaard, R. I., Wardle, J. F. C., & Roberts, D. H. 1990, *AJ*, 100, 1057
- Kollgaard, R. I., Wardle, J. F. C., & Roberts, D. H. 1994, in preparation
- Kollgaard, R. I., Wardle, J. F. C., Roberts, D. H., & Gabuzda, D. C. 1982, *AJ*, 104, 1687
- Kühr, H., Nauber, U., Pauliny-Toth, I. I. K., & Witzel, A. 1979, *MPIfR Preprint Nr55*
- Kühr, H., Stocke, J. T., Strittmatter, P. A., Eckart, A., Schalinski, C., Witzel, A., & Biermann, P. 1986, *ApJ*, 302, 52
- Kühr, H., Witzel, A., Pauliny-Toth, I. I. K., & Nauber, U. 1981, *A&AS*, 45, 367
- Landau, R., Epstein, E., & Rather, J. 1980, *AJ*, 85, 363
- Lind, K. R., & Blandford, R. D. 1985, *ApJ*, 295, 358
- Lonsdale, C. J., & Barthel, P. D. 1987, *AJ*, 94, 1487
- Murphy, D. 1993, private communication
- Murphy, D., Browne, I. W. A., & Perley, R. 1993, *MNRAS*, 264, 298
- Neff, S. G., & Hutchings, J. B. 1990, *AJ*, 100, 1441
- Neff, S. G., Hutchings, J. B., & Gower, A. C. 1989, *AJ*, 97, 1291
- O'Dea, C. P., Barvainis, R., & Challis, P. M. 1988, *AJ*, 96, 435
- Owen, F. N., & Mufson, S. L. 1977, *AJ*, 82, 776
- Owen, F. N., Porcas, R. W., Mufson, S. L. & Moffett, T. J. 1978, *AJ*, 83, 685
- Owen, F. N., & Puschell, J. J. 1984, *AJ*, 89, 932
- Owen, F. N., Spangler, S. R., & Cotton, W. D. 1980, *AJ*, 85, 351
- Padovani, P., & Urry, C. M. 1992, *ApJ*, 387, 449
- Pearson, T. J., Perley, R. A., & Readhead, A. C. S. 1985, *AJ*, 90, 738
- Pearson, T. J., & Readhead, A. C. S. 1988, *ApJ*, 328, 114
- Perley, R. A. 1982, *AJ*, 87, 859
- Perley, R. A., Fomalont, E. B., & Johnston, K. J. 1980, *AJ*, 85, 649
- Perley, R. A., Fomalont, F. B., & Johnston, K. J. 1982, *AJ*, 255, L93
- Steppe, H., Salter, C. J., Chini, R., Kreysa, E., Brunswig, W., & Perez, J. L. 1988, *A&AS*, 75, 317
- Simon, R. S., Johnston, K. J., & Spencer, J. H. 1985, *ApJ*, 290, 66
- Teräsanta, H., *et al.* 1992, *A&AS*, 94, 121
- Tornikoski, M., Valtaoja, E., Teräsanta, H., Lainela, M., Bramwell, D., & Bottl, L. C. L. 1993, *AJ*, 105, 1680
- Ulvestad, J. S. 1993, private communication
- Ulvestad, J. S., Johnston, K. J., & Weiler, K. W. 1983, *ApJ*, 266, 18
- Van Bruegel, W. J. M., Fanti, C., Fanti, R., Stanghellini, C., Schilizzi, R. T., & Spencer, R. E. 1992, *A&A*, 256, 56
- Veron-Cetty, M.-P., & Véron, P. 1991, *A Catalog of Quasars and Active Nuclei* (5th edition), ESO Scientific Report No. 10 (European Southern Observatory, Germany)
- Willis, D. 1979, *ApJS*, 39, 291
- Wiren, S., Valtaoja, E., Teräsanta, H., & Kotilainen, J. 1992, *AJ*, 104, 1009